NAVAL POSTGRADUATE SCHOOL
Monterey, California

THESIS

INVESTIGATION OF A HEAT DRIVEN
THERMOACOUSTIC PRIME MOVER
ABOVE ONSET OF SELF-OSCILLATION

by

Earl Clayton Bowers

September 1991

Thesis Advisor: Anthony A. Atchley
Co-Advisor: Felipe Gaitan

Approved for public release;
distribution is unlimited.

Unclassified

SECURITY CLASSIFICATION OF THIS PAGE

REPORT DOCUMENTATION PAGE

1a Report Security Classification: UNCLASSIFIED		1b Restrictive Markings	
2a Security Classification Authority		3 Distribution Availability of Report: Approved for public release; distribution is unlimited	
2b Declassification/Downgrading Schedule			
4 Performing Organization Report Number(s)		5 Monitoring Organization Report Number(s)	
6a Name of Performing Organization: Naval Postgraduate School	6b Office Symbol (*If Applicable*): PH	7a Name of Monitoring Organization: Naval Postgraduate School	
6c Address (*city, state, and ZIP code*): Monterey, CA 93943-5000		7b Address (*city, state, and ZIP code*): Monterey, CA 93943-5000	
8a Name of Funding/Sponsoring Organization	8b Office Symbol (*If Applicable*)	9 Procurement Instrument Identification Number	
8c Address (*city, state, and ZIP code*)		10 Source of Funding Numbers: Program Element Number / Project No / Task No / Work Unit Accession No	

11 Title (*Include Security Classification*): Investigation of a Heat Driven Thermoacoustic Prime Mover above Onset of Self-Oscillation

12 Personal Author(s): Bowers, Earl Clayton

13a Type of Report	13b Time Covered	14 Date of Report (*year, month, day*)	15 Page Count
Master's Thesis	From To	September 1991	63

16 Supplementary Notation: The views expressed in this thesis are those of the author and do not reflect the official policy or position of the Department of Defense or the U.S. Government.

17 Cosati Codes			18 Subject Terms (*continue on reverse if necessary and identify by block number*)
Field	Group	Subgroup	Acoustics, Thermoacoustics, Prime Mover, Thermoacoustic Heat Transport

19 Abstract (*continue on reverse if necessary and identify by block number*)

The goal of this thesis is to investigate the work output of a heat driven thermoacoustic prime mover above onset of self-oscillation. The exponentially growing sound wave, generated when a prime mover is initially "turned on," was digitally sampled for a helium filled prime mover at pressures ranging from 238 kPa to 500 kPa and at temperature differences ranging from onset to 400 K. This data was then digitally filtered by a 100 Hz band pass filter centered on the prime mover's fundamental frequency. A least mean squares fit was applied to the envelope of the filter's output in order to determine the temporal absorption coefficient β. From β, the quality factor was computed. These quality factors were then compared to thermoacoustic theory. The agreement between the theoretical predictions and the measured results is extremely good at high mean gas pressures. As the mean gas pressure decreases, however, the agreement between the theoretical value of onset and the predicted slope of the data, increasingly deviate.

20 Distribution/Availability of Abstract	21 Abstract Security Classification	
[X] unclassified/unlimited [ ] same as report [ ] DTIC users	Unclassified	
22a Name of Responsible Individual: Anthony A. Atchley	22b Telephone (*Include Area code*): (408) 646-2848	22c Office Symbol: PH/Ay

DD FORM 1473, JUN 86 *Previous editions are obsolete.* S/N 0102-LF-014-6603

SECURITY CLASSIFICATION OF THIS PAGE Unclassified

Approved for public release; distribution is unlimited.

Investigation of a Heat Driven Thermoacoustic Prime Mover above Onset of Self-Oscillation

by

Earl Clayton Bowers
Lieutenant, United States Navy
B.S., United States Naval Academy, 1985

Submitted in partial fulfillment
of the requirements for the degrees of

MASTER OF SCIENCE IN APPLIED SCIENCE, and
MASTER OF SCIENCE IN ENGINEERING ACOUSTICS

from the

NAVAL POSTGRADUATE SCHOOL
September 1991

ABSTRACT

The goal of this thesis is to investigate the work output of a heat driven thermoacoustic prime mover above onset of self-oscillation. The exponentially growing sound wave, generated when a prime mover is initially "turned on," was digitally sampled for a helium filled prime mover at pressures ranging from 238 kPa to 500 kPa and at temperature differences ranging from onset to 400 K. This data was then digitally filtered by a 100 Hz band pass filter centered on the prime mover's fundamental frequency. A least mean squares fit was applied to the envelope of the filter's output in order to determine the temporal absorption coefficient β. From β, the quality factor was computed. These quality factors were then compared with thermoacoustic theory. The agreement between the theoretical predictions and the measured results is extremely good at high mean gas pressures. As the mean gas pressure decreases, however, the agreement between the theoretical value of onset and the predicted slope of the data, increasingly deviate.

TABLE OF CONTENTS

I. INTRODUCTION

As thermoacoustics is a relatively new technology, its potential uses are still being investigated. One such use, which this thesis intends to precede, is the use of a thermoacoustic prime mover as a low frequency transducer. This possibility has been discussed by S. L. Garrett and T. B. Gabrielson as a viable alternative to the conventional sound sources used today.

For conventional sources, the motion of a solid surface is required to generate a volumetric velocity. The pressure amplitude is consequently limited by the maximum displacement of the solid. The relationship between the pressure amplitude P and the angular frequency of oscillation ω for a spherical source in an infinite medium is

$$P = Q\frac{\rho a}{2\lambda r} = Q\frac{\rho\omega}{4\pi r}, \tag{1}$$

where the volumetric velocity Q is given by

$$Q = \int_{surface} \mathbf{v}\cdot\mathbf{n}\,dA. \tag{2}$$

Also, ρ is the density of the medium, a is the speed of sound in the medium, λ is the wavelength of the oscillating wave, r is the range from the source, and $\mathbf{v}$, $\mathbf{n}$, and A are the surface

velocity, the unit vector normal to the surface, and the surface area of the source, respectively. Assuming sinusoidal oscillations, the surface velocity can be expressed as $v = \omega d$, where d is the displacement of the surface. Consequently Q is proportional to ω, the pressure amplitude to ω^2, and the radiated acoustic power to ω^4. As a result, as frequency is decreased, the surface area must be increased quadratically in order to maintain a constant pressure amplitude in the far field ($P \propto \omega^2 \cdot A$). Thermoacoustics offers a solution to this problem because the driving force can be applied directly to the fluid instead of through an oscillating surface. With only fluid motion, the limitation to the velocity no longer comes from the elastic constraints of a vibrating solid but from the hydrodynamic (e.g., turbulence) limits of the fluid. (Garrett et al., 1990, pp. 162-163) The actual phenomenon of thermoacoustics has been discussed at length elsewhere. G. W. Swift's 1988 article "Thermoacoustic engines", for example, gives a very thorough coverage of the subject. It therefore will not be explained in this thesis.

Thermoacoustics research at the Naval Postgraduate School has been directed at thoroughly verifying thermoacoustic theory. In 1989, Hsiao-Tseng Lin studied a thermoacoustic prime mover below onset (Lin, 1989). The conclusions of his thesis indicated that theory based on short-stack and boundary layer approximations did not hold valid in all cases. He also

found that above onset, the acoustic amplitude quickly became quite large, and the waveforms highly nonlinear.

The next logical progression in this research is to study a prime mover above onset while the acoustic amplitude is small and to apply a non short stack, boundary layer theory. It is intended that the information gained will help lead to an understanding of prime movers at large amplitudes. The purpose of this thesis is to take the first step by looking at the initial growth of the oscillations as they build up to steady state.

II. THEORY

A. INTRODUCTION

A prime mover can be divided into five major regions. These five regions, as shown in Figure 1, are the ambient end, the ambient heat exchanger, the stack, the hot heat exchanger, and the hot end. In typical configurations, the ambient and hot ends are empty capped tubes maintained at constant temperature. Since we chose to apply a differential temperature to the prime mover by heating one end while keeping the other end at ambient temperature, hot and ambient are used to describe the different regions. The ambient and hot heat exchangers both consist of a series of plates used to maintain the opposing ends of the stack region at their respective temperatures. Finally, the stack region is where the conversion of thermal to acoustic energy takes place.

The purpose of this thesis is to compare the measured work output of a prime mover above onset of self-oscillation to the theoretical value. Unfortunately, it is not a simple matter to directly measure the work output. What is easily measured though, is the acoustic signal generated by the prime mover. The evolution of this signal can be related to the work output as discussed below.

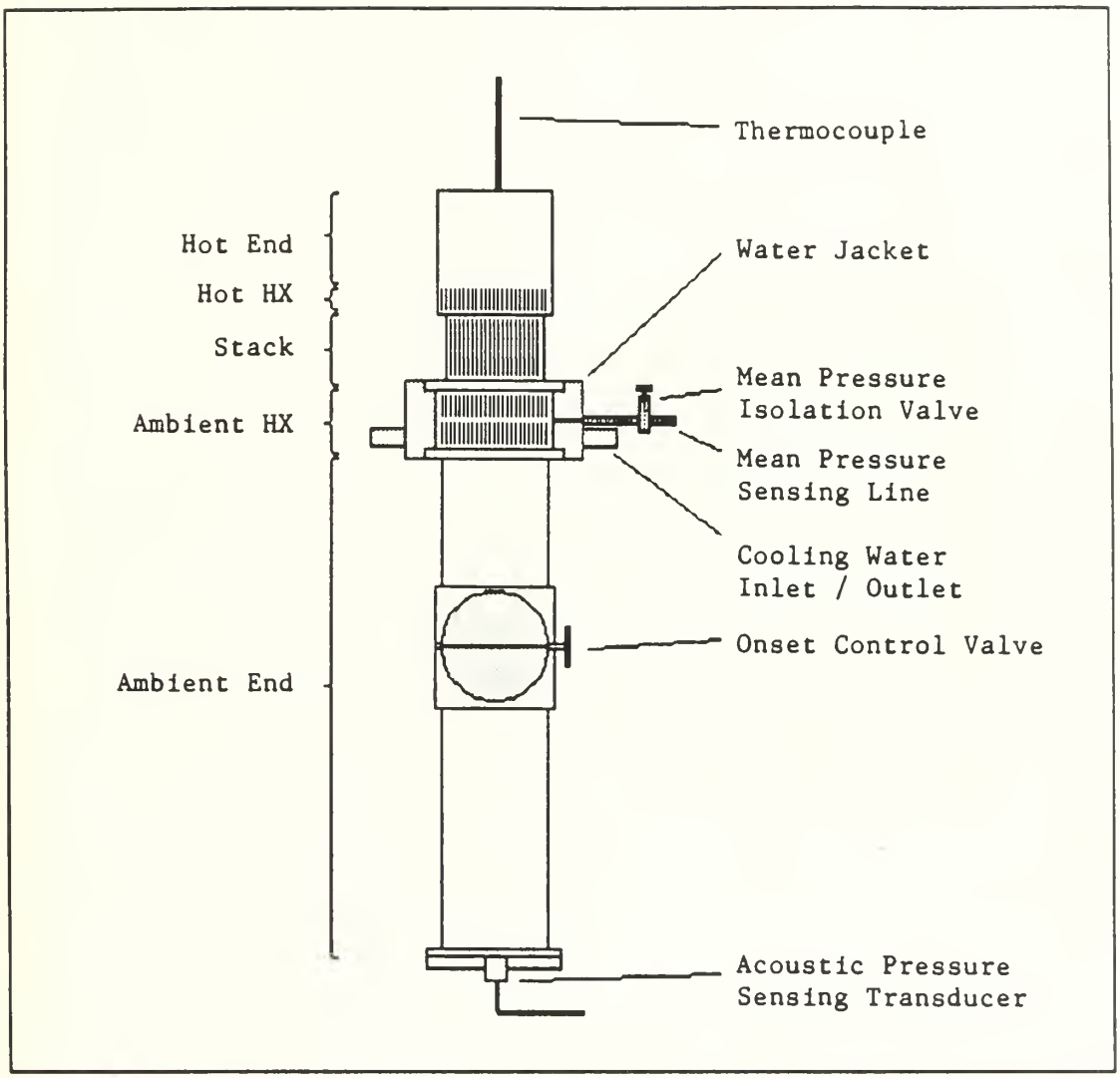

Figure 1 Major regions and components of a prime mover.

When a resonator is excited and then allowed to decay, the amplitude of the oscillations decay according to

$$e^{-\omega t/2Q} e^{j\omega t}, \tag{3}$$

where t is time, Q is the quality factor of the resonator and $j^2 = -1$. (Swift, 1988, p. 1162) In terms of the temporal absorption coefficient β, this exponential behavior is

$$e^{-\beta t} e^{j\omega t}, \tag{4}$$

where $\beta = \omega/2Q$. The initial buildup of oscillations in a prime mover can be characterized by a negative value of β. Thus, the amplitude initially grows exponentially. As the oscillations become larger in amplitude, however, the value of the net absorption coefficient changes and eventually equals zero. This results in steady state oscillations of finite amplitude as can be seen in Figure 2. It is the initial growth of the signal that is of interest to us.

β, which is equivalent to the inverse of the rise time, can be directly obtained from analyzing the envelope of the acoustic signal generated by the prime mover. Along with β, the frequency of oscillation is also measured so that 1/Q may be computed. Recall that $1/Q = 2\beta/\omega = \beta/\pi f$, where f is the oscillation frequency measured in hertz. The choice of using 1/Q as the parameter of interest comes from the fact that it

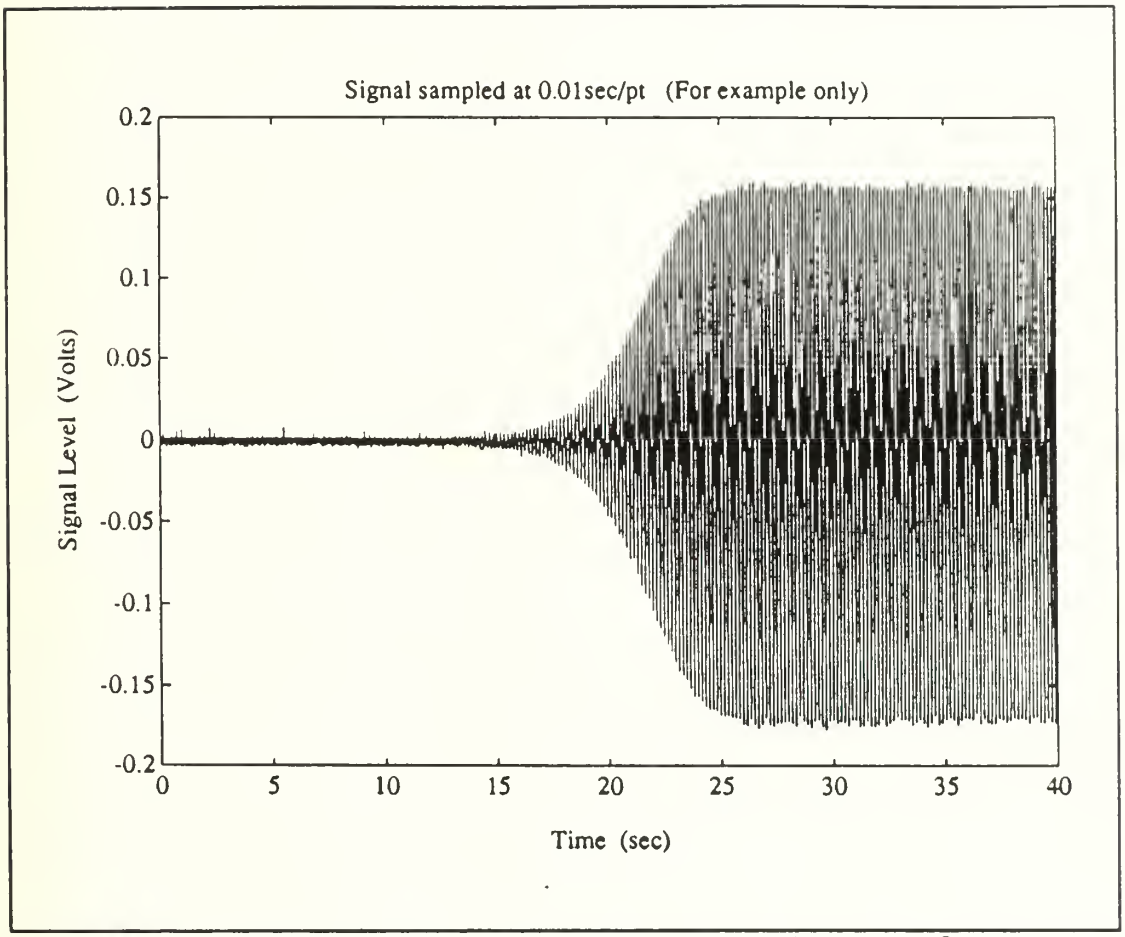

Figure 2 Signal which shows the changing of β from an initial negative value (evidenced by the exponential buildup), to zero (as indicated by the steady state result).

is directly proportional to the work output of the prime mover. As discussed by Swift, 1/Q relates to the average dissipated acoustic power $\dot{E}$ of a prime mover by

$$\frac{1}{Q} = \frac{\dot{E}}{\omega E_{ST}}, \tag{5}$$

where E_{ST} is the energy stored in the resonator (Swift, 1988, p. 1162). Rather than using the dissipated acoustic power $\dot{E}$, we prefer to work with the generated acoustic power $\dot{W}$. $\dot{W}$ is commonly referred to as the work output. By convention, $\dot{W}$ is positive when power is generated while $\dot{E}$ is positive when power is dissipated. Therefore, $\dot{E} = -\dot{W}$, and

$$\frac{1}{Q} = \frac{-\dot{W}}{\omega E_{ST}}. \tag{6}$$

B. AVERAGE GENERATED ACOUSTIC POWER, $\dot{W}_{stack}$

The acoustic power generated in the stack section of a prime mover cannot flow or escape in a direction perpendicular to the stack plates, the y-direction. Energy transport is allowed however, in the x-direction which is parallel to both the plates and the temperature gradient. A measurement of the difference in average acoustic intensity between the two ends of the stack can therefore be used to determine the acoustic power generated by the stack.

The acoustic power generated by a short segment of stack is given by

$$\dot{W}_{stack} = S[(\overline{pu})_{\substack{right\\ end\ of\\ segment}} - (\overline{pu})_{\substack{left\\ end\ of\\ segment}}] = S\Delta x \frac{d}{dx}(\overline{pu}) \tag{7}$$

where S is the cross sectional area of the fluid in the stack, $\overline{pu}$ is the time average acoustic intensity, and Δx is the length of the short segment. Note that $S\Delta x$ is the total volume of the fluid in the stack region. By dividing through by this volume, the power per unit volume is obtained;

$$\dot{w} = \frac{\dot{W}_{stack}}{S\Delta x} = \frac{d}{dx}(\overline{pu}) = \frac{1}{2} Re[p_1 \frac{d\langle \tilde{u}_1 \rangle}{dx} + \frac{dp_1}{dx}\langle \tilde{u}_1 \rangle], \tag{8}$$

where a tilde denotes complex conjugate, and p_1 and u_1 represent the spatial dependence of the pressure and velocity, respectively, (i.e. $p(x,t) = p_1 e^{j\omega t}$ and $u(x,t) = u_1 e^{j\omega t}$). Also, the angled brackets denote the spatial average of velocity across the fluid gap between the plates. It is necessary to spatially average the acoustic velocity across the fluid gap because, with the presence of viscosity, u is also y-dependent. Expressions for the four terms on the right hand side of this equation will be derived next in order to arrive at a complete equation for work output. (Swift, 1988, p. 1159)

Since the prime mover is essentially a pipe with rigid ends, the pressure behaves sinusoidally like a cosine wave.

$$p_1 = P_A \cos(kx), \tag{9}$$

where P_A is the peak pressure amplitude, k is the wave number, and x = 0 at the capped end of the ambient end.

Similarly, it can be shown that the velocity in the stack is represented by

$$u_1 = -j\frac{P_A}{\rho_m a}\left(1 + \frac{l}{y_o}\right)\sin(kx) \equiv j u_1^s, \tag{10}$$

where ρ_m is the mean density of the fluid, l is one-half the plate thickness, and y_o is one-half the plate spacing. (Swift, 1988, p. 1157)

From the equation of motion for a compressible, viscous fluid, Swift has shown that

$$\frac{dp_1}{dx} = \frac{-j\omega\rho_m \langle u_1 \rangle}{1 - f_v} = \frac{\omega\rho_m \langle u_1^s \rangle}{1 - f_v}, \tag{11}$$

where

$$f_v = \frac{\tanh[(1 + j)y_o/\delta_v]}{(1 + j)y_o/\delta_v} \tag{12}$$

and $\delta_\upsilon = \sqrt{2\mu/\rho\omega}$ is the fluid's viscous penetration depth and μ is the dynamic viscosity of the fluid (Swift, 1988, p. 1159).

Finally, the wave equation can now be used to solve for $d\langle u_1\rangle/dx$. (Swift, 1988, p. 1157)

$$\left(1 + \frac{(\gamma-1) f_\kappa}{1 + \epsilon_s}\right) p_1 + \frac{\rho_m a^2}{\omega^2} \frac{d}{dx}\left(\frac{1 - f_\upsilon}{\rho_m} \frac{dp_1}{dx}\right) - \frac{a^2}{\omega^2} \frac{f_\kappa - f_\upsilon}{(1 - \sigma)(1 + \epsilon_s)} \frac{\nabla T_m}{T_m} \frac{dp_1}{dx} = 0 \tag{13}$$

where

$$\epsilon_s = \frac{\rho_m c_p \delta_\kappa \tanh[(1 + j) y_o/\delta_\kappa]}{\rho_s c_s \delta_s \tanh[(1 + j) l/\delta_s]}, \tag{14}$$

c_p and c_s are the isobaric specific heats per unit mass for the fluid and the solid (i.e. the plate), $\delta_\kappa = \sqrt{2K/\rho_m c_p \omega}$ and $\delta_s = \sqrt{2K_s/\rho_s c_s \omega}$ are the thermal penetration depths in the fluid and the solid, ρ_s is the density of the solid, and K and K_s are the thermal conductivity of the fluid and the solid. Also, γ is ratio of the fluid's isobaric to isochoric specific heats, σ is the fluid's Prandtl number, ∇T_m is the mean-temperature gradient in the x-direction, T_m is the mean temperature, and f_κ is a function similar to f_υ. Substituting Eq. (11) into the second term of the wave equation yields the following;

$$\frac{d\langle u_1 \rangle}{dx} = j\frac{1}{\omega\rho_m}\frac{f_\kappa - f_\nu}{(1-\sigma)(1+\epsilon_s)}\frac{\nabla T_m}{T}\frac{dp_1}{dx} - j\frac{\omega}{\rho_m a^2}\left(1 + \frac{(\gamma-1)f_\kappa}{1+\epsilon_s}\right)p_1. \tag{15}$$

Applying these four expressions, Eqs. (9), (10), (11), and (15), to Eq. (8) gives the equation we have been working for;

$$\dot{w} = \frac{1}{2}Re\left[\frac{P_A^2\omega}{\rho_m a^2}\left[j\left(\frac{\tilde{f}_\kappa - \tilde{f}_\nu}{1-\tilde{f}_\nu}\frac{1+\frac{1}{y_o}}{(1-\sigma)(1+\epsilon_s)}\frac{\nabla T_m}{kT_m}\tan(kx) + 1 + \frac{\gamma-1}{1+\epsilon_s}\tilde{f}_\kappa\right)\cos^2(kx) - j\frac{(1+\frac{1}{y_o})^2}{1-f_\nu}\sin^2(kx)\right]\right]. \tag{16}$$

Now with $\dot{w}$ known, computing the total acoustic power simply requires integrating over the volume of the fluid within the stack;

$$\dot{W}_{stack} = \int \dot{w}dV = \int \dot{w}Sdx. \tag{17}$$

C. TOTAL ACOUSTIC POWER, $\dot{W}$

To compute 1/Q, the total acoustic power $\dot{W}$ is needed. In the previous section, only an expression for the work done by the prime mover's stack was derived. The four remaining

sections of the prime mover also need to enter into the equation. The total work done by the prime mover can be divided into the sum of the work done by or on each of these five individual sections,

$$\dot{W} = \dot{W}_{amb\ end} + \dot{W}_{amb\ hx} + \dot{W}_{stack} + \dot{W}_{hot\ hx} + \dot{W}_{hot\ end}. \qquad (18)$$

It should be noted that, with the exception of $\dot{W}_{stack}$, these terms represent losses. $\dot{W}_{stack}$ can represent either loss or gain depending on the value of the temperature gradient.

The equation for $\dot{w}$ was derived for the stack region but it actually applies to each of the remaining four regions. The parameters in $\dot{w}$ simply vary depending on what section of the prime mover x happens to be in. In all four remaining regions for example, $\nabla T_m = 0$ since there is no temperature gradient anywhere except in the stack region. Likewise, $1 = 0$ in the ambient and hot ends since these regions do not contain any plates and the functions f_v and f_κ take on slightly different forms as well.

The total acoustic power is consequently one integral from the beginning of the ambient end to the end of the hot end,

$$\dot{W} = \int_{x=0}^{L} \dot{w}(x)\, S(x)\, dx. \qquad (19)$$

Within this integral numerous parameters vary with respect to x depending upon which region of the prime mover x happens to

be in (e.g., perimeter size, plate thickness, plate spacing). Also, within the given region of the stack there are several parameters which vary as a function of x because of the temperature change along the stack (e.g., sound speed, thermal conductivity of the fluid, viscosity, etc.). All such parameters are treated as functions of x so that a single integration yields the total work done by the prime mover.

D. STORED ENERGY, E_{ST}

The final quantity needed to calculate 1/Q is the energy stored in the resonator. This is found by integrating the time averaged energy density over the volume of the resonator.

$$E_{ST} = \int \overline{\mathscr{E}_i} dV, \tag{20}$$

where the instantaneous energy density is given by

$$\mathscr{E}_i = \frac{1}{2}\rho_m \left(\frac{p^2}{\rho_m^2 a^2} + u^2 \right), \tag{21}$$

and its time average by

$$\overline{\mathscr{E}_i} = \frac{1}{4}\frac{p_1^2}{\rho_m a^2} + \frac{1}{4}\rho_m (u_1^s)^2. \tag{22}$$

Again, as in the case of acoustic power, the total stored energy can be represented as the sum of the stored energy in each of the prime mover's five regions,

$$E_{ST} = E_{ST_{amb\ end}} + E_{ST_{amb\ hx}} + E_{ST_{stack}} + E_{ST_{hot\ hx}} + E_{ST_{hot\ end}}. \qquad (23)$$

Choosing appropriate expressions for p_1 and u_1, and integrating the time averaged energy density over each of the five regions produces:

$$\begin{aligned} E_{ST} = \frac{1}{4}\frac{P_A^2 S}{\rho_m a^2}\Bigg[& x_{amb\ end} \\ & + \int_{amb\ hx}\left[\frac{\cos^2(kx+\phi)}{1+\frac{1}{y_o}} + \left(1+\frac{1}{y_o}\right)\sin^2(kx+\phi)\right]dx \\ & + \int_{stack}\left[\frac{\cos^2(kx+\phi)}{1+\frac{1}{y_o}} + \left(1+\frac{1}{y_o}\right)\sin^2(kx+\phi)\right]dx \\ & + \int_{hot\ hx}\left[\frac{\cos^2(kx+\phi)}{1+\frac{1}{y_o}} + \left(1+\frac{1}{y_o}\right)\sin^2(kx+\phi)\right]dx \\ & + x_{hot\ end}\Bigg] \end{aligned} \qquad (24)$$

where ϕ is the phase of the standing wave at the entrance of the region. Finally, combining Eqs. (16), (19) and (24) with Eq. (6) yields the desired parameter, 1/Q.

III. EXPERIMENTAL SETUP

A. THE PRIME MOVER TUBE

The physical construction of the prime mover assembly was previously shown in Figure 1. Its internal diameter is 3.82 cm and its overall internal length is 1.0005 m. A complete listing of all important prime mover measurements is found in Appendix A.

1. The Hot Heat Exchanger and the Hot End

The hot heat exchanger and the hot end tube are both constructed of nickel as is the end-cap of the hot end tube. This end-cap is welded to the hot end tube and presents a rigid boundary for sound waves generated by the prime mover. Through the center of this end-cap a small hole has been drilled to accommodate a thermocouple probe for sensing the hot heat exchanger temperature. To prevent leakage of gas through this hole, the thermocouple probe is epoxied in place.

The hot end tube is 0.63 cm thick and has an internal length of 5.50 cm. Its internal diameter, as are all of the individual components which make up the prime mover, is 3.82 cm. The hot heat exchanger assembly consists of 25, 0.045 cm thick and 0.762 cm long nickel plates. The spacing between each plate is 0.104 cm. To minimize deformation from high temperatures, spacers made from 304 stainless steel with a

diameter of 0.031 cm are welded to one side of each plate. The hot heat exchanger assembly is mounted to the open end of the hot end tube.

2. The Stack

The prime mover stack is housed in a 304 stainless steel tube of 0.05 cm thickness with a length of 3.50 cm. It is comprised of 35, 0.028 cm thick 304 stainless steel plates and is the same length as the tube. The plate spacing in the stack region is 0.077 cm and, as in the hot heat exchanger, spacers are attached to each plate to minimize deformation. The stack and the hot heat exchanger are assembled such that their plates are at near right angles to one another so that the plates of the heat exchanger do not coincide with the gaps in the stack. Such a misalignment would result in the blockage of fluid flow.

3. The Ambient Heat Exchanger and Ambient End

The ambient heat exchanger consists of two identical copper stacks each containing 25, 1.02 cm long, 0.045 cm thick plates. The gap between each plate is 0.104 cm and the spacing between the two individual stacks is 0.15 cm. These two stacks are housed within a brass water jacket and the hot end/stack assembly is soldered to one end of the jacket. The other end of the jacket is soldered to the ambient end of the prime mover which is constructed of an 88.11 cm long copper tube. A butterfly valve is positioned within this tube, 38 cm

from the ambient heat exchanger. The purpose of this valve is to shut off the sound wave generated by the prime mover. By closing the valve the internal length of the prime mover is effectively shortened requiring a much higher differential temperature to drive the prime mover above onset. In this way, a differential temperature which places the prime mover above onset can be established without sound being generated. By opening the valve the prime mover is instantaneously placed above onset (turned on) and the initial pressure wave build up may be observed and measured. Lastly, the ambient end is flanged and a brass end-cap which houses a pressure sensing transducer is fastened to it.

B. CONTROL AND MEASUREMENT EQUIPMENT

1. Temperature

The temperature of the hot heat exchanger is controlled by an Omega Engineering HBA Model 202040 heater powered by a GR Type 100-Q variable transformer. The heater coils are tightly wrapped and cover the entire hot end and hot heat exchanger assembly to provide a constant "hot" temperature to this portion of the prime mover. As previously mentioned, a type K thermocouple entering through the hot end end-cap is positioned in contact with the hot heat exchanger to measure the hot end temperature. During operation the hot end assembly is surrounded with insulation to minimize heat loss.

Ambient end temperature is controlled through the use of a Neslab RTE-110 constant temperature bath. The bath is used to cycle constant temperature water through the water jacket surrounding the ambient heat exchanger and then through plastic tubing which is wrapped around the entire length of the ambient end. Temperature is monitored via three type E thermocouples which are glued to the top, middle, and bottom sections of the ambient end. This method of ambient temperature control maintains the ambient end temperatures within a 1°C spread. The hot end thermocouple along with the three ambient end thermocouples are monitored using a Keithley 740 System scanning thermometer.

2. Pressure

Mean pressure inside the prime mover is sensed via a connection which penetrates the prime mover between the two ambient heat exchanger stacks. This connection is valved so that the pressure sensing line may be isolated from the prime mover when oscillations are being measured. Leaving the valve open increases the losses of the prime mover and actually puts it below onset for the differential temperatures examined. Pressure is measured from this sensing line by an Omega PX304-300AV pressure transducer and an HP-3478A multimeter is used to display the voltage output of the transducer. Pressurizing the prime mover is done by first evacuating the prime mover

chamber with a vacuum pump and then filling it with helium gas. All this is done via the pressure sensing line.

3. Signal

The acoustic signal generated by a differential temperature applied to the prime mover is sensed by an ENDEVCO Model 8510B-5 piezoresistive pressure transducer housed within the ambient end end-cap. The linear response range of the transducer is ±5 psi. A high impedance leak is provided between the resonator and the back volume of the transducer to eliminate the dc pressure difference on the transducer while having negligible effect on the acoustic pressure differences. The leak is a 0.004" internal diameter, approximately 10 cm long piece of copper-nickel capillary tubing. The signal from the transducer is routed through a locally constructed differential amplifier which boosts the signal by a factor of ten. This amplified signal is then applied as input to a Nicolet 310 digital oscilloscope for data collection and storage.

IV. EXPERIMENTAL PROCEDURE AND SIGNAL PROCESSING

A. DATA COLLECTION

The first step in obtaining prime mover response data was to evacuate the resonator. This was accomplished by pumping down the prime mover via its pressure sensing line for several hours. Once fully evacuated, the vacuum pump was turned off and isolated from the prime mover. The tube's internal pressure was then recorded and this value was used as the calibration value for the pressure sensor. All future pressure readings were corrected by this amount. The prime mover was then filled with the desired pressure of helium to within a tolerance of ± 1 kPa.

For temperature control, the constant temperature bath was started and the variable transformer was turned up to power the heater element. Once a steady state differential temperature of interest was reached, the prime mover was ready for data collection.

As mentioned previously, a Nicolet 310 digital oscilloscope (NIC-310) was used to sample the waveform generated by the prime mover. Since the data was being digitally sampled it was important to at least satisfy the Nyquist sampling rate of $2f_{max}$ in order to prevent aliasing, where f_{max} is the highest frequency of interest (Strumm, 1988,

p. 54). For the prime mover, we are only concerned with the rise time of the fundamental component of the acoustic signal which has a frequency of approximately 500 Hz. Consequently we must sample at a minimum of 1000 Hz. To be conservative a sampling frequency of four times the fundamental was chosen as the minimum acceptable sampling frequency. As it turns out, the closest sampling frequency offered by the NIC-310 without violating this threshold is 5000 Hz or 200 μs per data point. With the 4000 point data capacity of the NIC-310, this process enabled the recording of sample records of up to 0.8 seconds in duration.

Data collection was done by placing the onset control valve in the closed position to turn off the sound generated by the tube. After thermal equilibrium was achieved, the valve was opened. When a signal could be seen over the background noise present, the oscilloscope record was frozen and saved on a 3.5" floppy disk for later analysis. Several such records were taken for each pressure and temperature combination of interest.

B. DIGITAL SIGNAL PROCESSING

Analysis of the accumulated data was done with MathWorks' program MATLAB. The actual data records stored by the NIC-310, however, were in binary code so, to make the data records ready for processing, they were simply converted into ASCII files.

Initially, for each data record, a Discrete Fourier Transform (DFT) was computed and the fundamental frequency of the record was identified. This frequency was then used to translate the frequency spectrum of the signal so that the fundamental frequency was now located in the first bin of the DFT. This was accomplished by multiplying the signal by a complex exponential in the following fashion;

$$x_{new}(n) = e^{j(2\pi/N)Mn} x_{old}(n), \qquad (25)$$

where N is the number of points contained in the data record, n is an integer denoting the position within a record, and M is the number of bins which every frequency bin in the DFT of $x_{old}(n)$ is to be circularly shifted. For example, if the fundamental frequency of the DFT of $x_{old}(n)$ resides in bin M + 1, then a DFT of $x_{new}(n)$ will have the fundamental frequency located in its first bin. (Strumm, 1988, p. 429) The DFT of a typical data set is displayed in Figure 3. Note that there are two peaks in this DFT. This is because it is the DFT of a real (non complex) signal. Since real signals are sinusoidal, (i.e. the sum of two exponential functions of equal magnitude, but with frequencies of opposite sign), two fundamental frequencies result. One represents the positive frequency of the sine wave, the first half of the DFT, and the

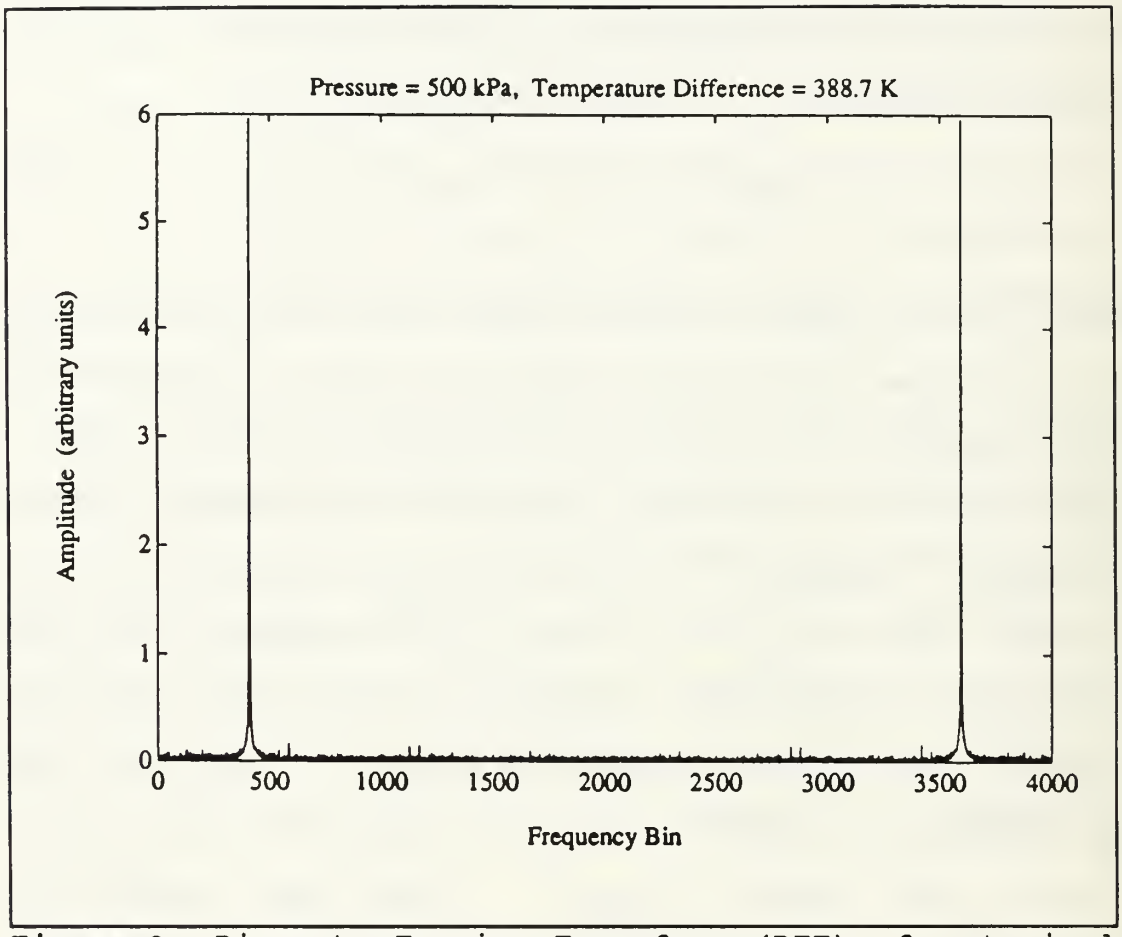

Figure 3 Discrete Fourier Transform (DFT) of a typical data record showing the presence of a 500 Hz signal.

other represents the negative frequency of the sine wave, the second half of the DFT.

Now, with the fundamental frequency effectively translated to dc level (first bin), a low pass filter can be applied to isolate the desired signal. The low pass digital filter chosen for this task was a fifth order Butterworth filter with a bandwidth of 50 Hz. This procedure is essentially the same as filtering the original data with a 100 Hz band pass filter centered at the fundamental frequency of the data record. By translating the data first, however, we immediately arrive at the envelope of the waveform since its frequency has been "converted" to dc. Figures 4 and 5 show a typical data record before and after processing, respectively. Note that processing the signal in this manner has the effect of halving the magnitude of the original signal.

In most cases the 4000 point DFT revealed that only the fundamental frequency was present. As the prime mover was driven higher (~50K) above onset, however, the second and even the third harmonics were observed. To ensure that only the affects caused by the fundamental were measured, DFT's were taken of the earliest parts of these data records to eliminate the second harmonic. This is important because, as the second and higher harmonics begin to grow, they take energy away from the first harmonic and cause β to change. Such losses are not accounted for by our theory. This effect can be seen in

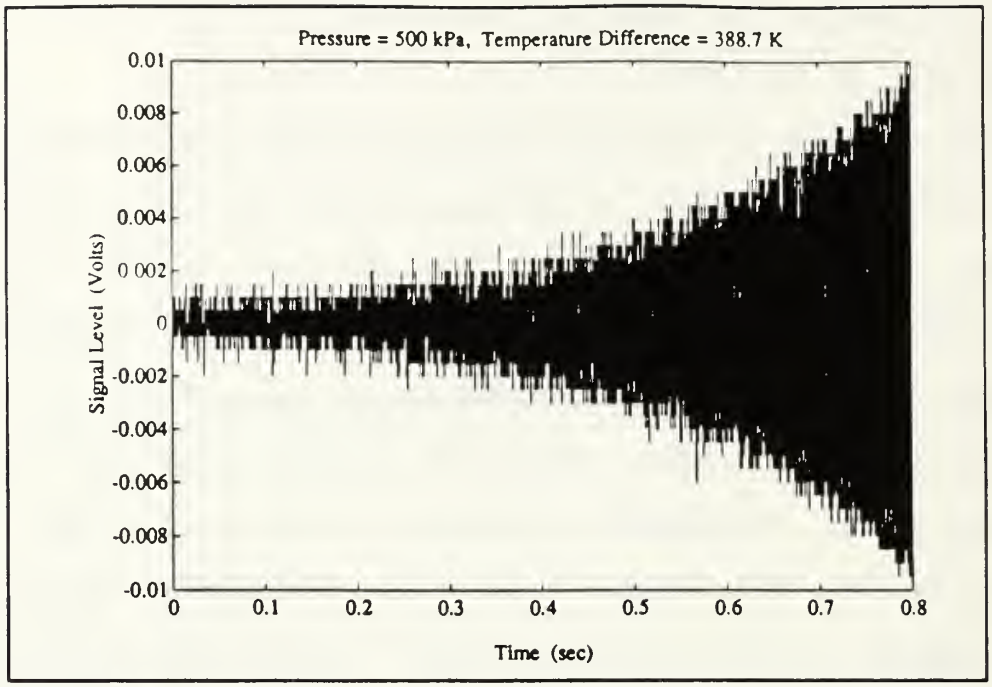

Figure 4 Typical data record before processing (Sampled at 5000 samples per second.)

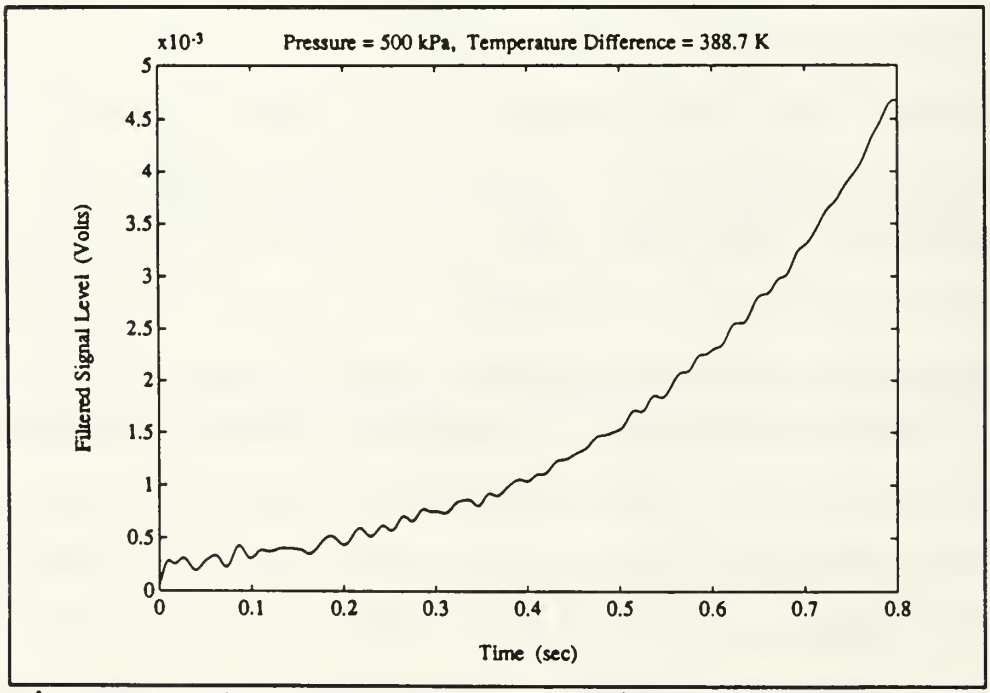

Figure 5 The result of processing the data record shown in Figure 4 above.

Figures 6 and 7 where the first 2000 data points contain only the fundamental frequency while the entire 4000 point sample shows evidence of the first three harmonics. Note that for the first 0.4 seconds (2000 samples), the slope of the logarithm of the envelope is essentially constant (Figure 7). This slope is equivalent to β since $d\beta/dt$ is approximately zero. As the harmonics begin to appear, however, the magnitude of β noticeably decreases as indicated by the lessening of the slope on the logarithmic plot of the data. The 2000 and 4000 point DFT's of this data are shown in Figures 8 and 9.

As with all digital filtering, the end conditions are the most difficult to match. Because of this the initial and final points of a filtered signal need to be discarded. To determine the actual range of the filtered data points which are "influenced" by the filtering process, test signals were generated of the following form;

$$TestSignal = 0.001\, e^{\beta t} \sin(2\pi\, 500 t). \qquad (26)$$

The use of a scaling factor of 0.001 and a frequency of 500 Hz were made to generate signals which were characteristic of the data being analyzed. Likewise, varying values of β were used to cover the range of β's that were being measured. The results show that smaller values of β produce larger relative fluctuations in the filtered waveform. Figures 10 and 11 show

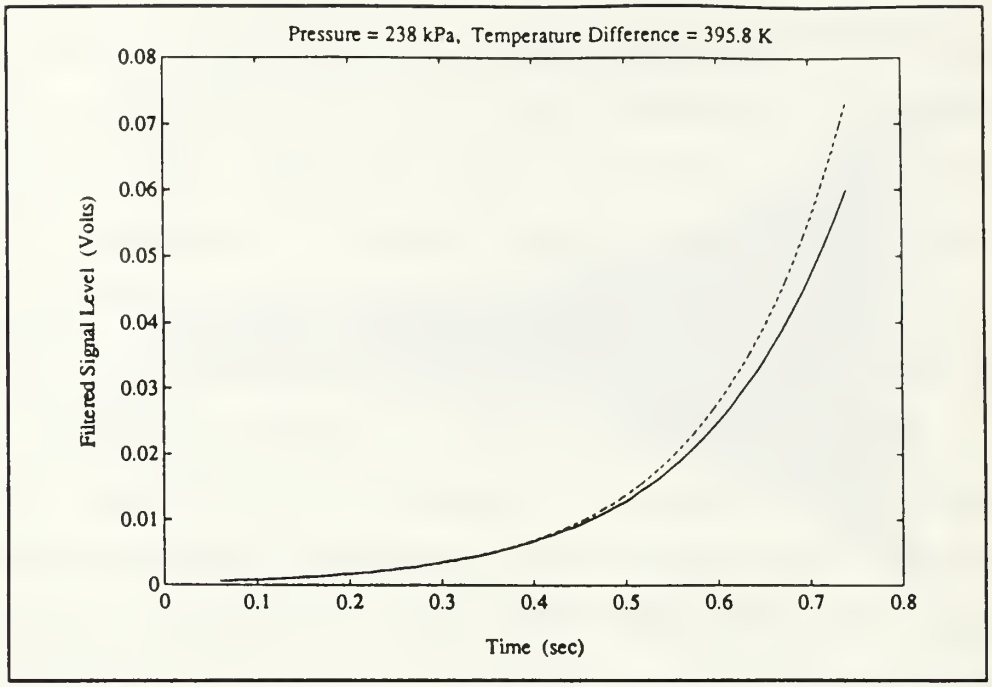

Figure 6 Filtered signal (solid line) which experiences the growth of higher harmonics after the first 0.4 seconds. The dashed line is a least mean squares fit to the first 0.4 seconds of data.

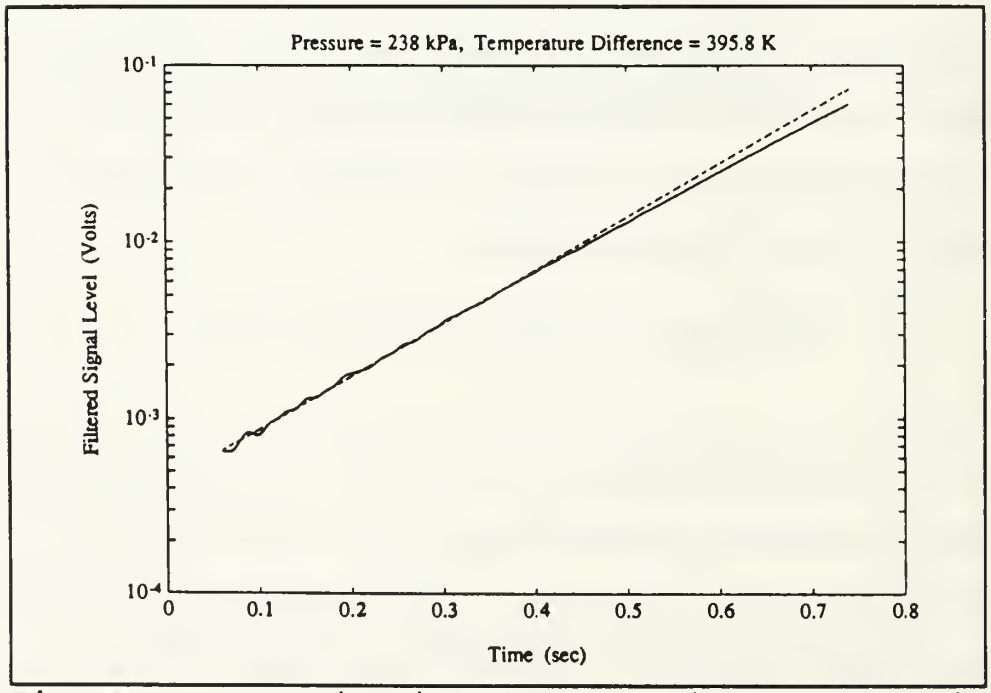

Figure 7 Logarithmic plot of signal shown in Figure 6 (solid line). The dashed line is a least mean squares fit to the first 0.4 seconds of data.

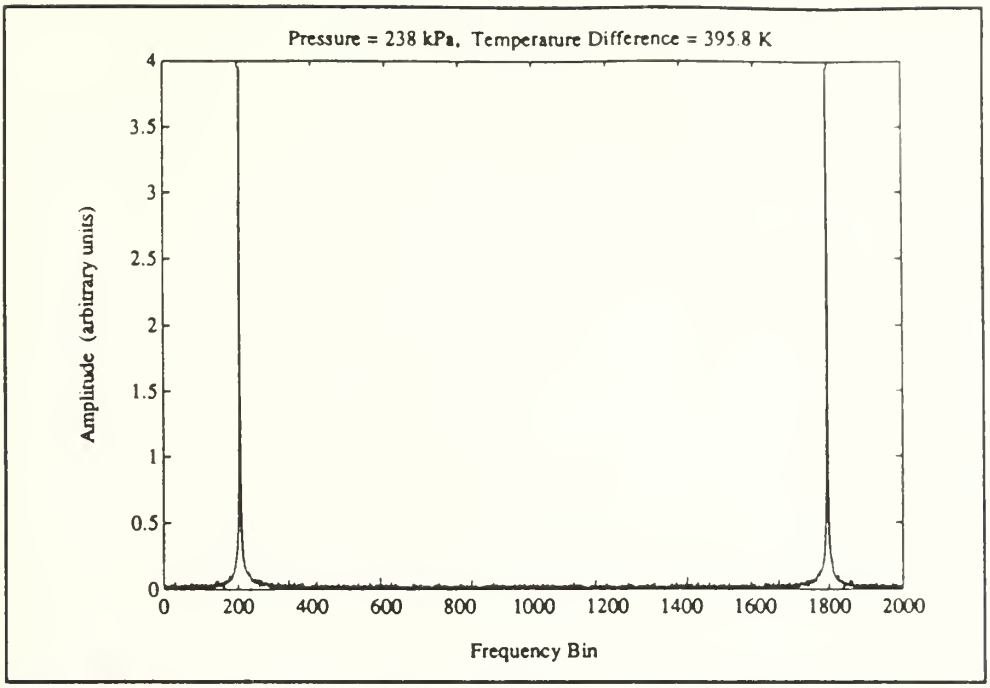

Figure 8 A 2000 point DFT of the signal shown in Figures 6 and 7, showing that only the fundamental frequency is present in the first 0.4 seconds of the signal.

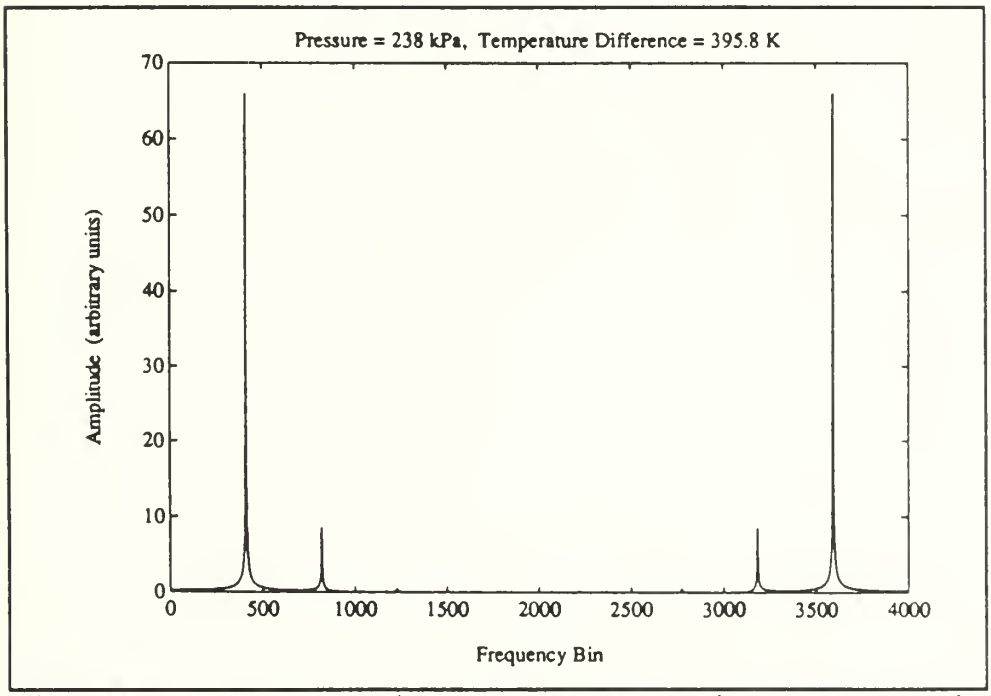

Figure 9 A 4000 point DFT of the signal shown in Figures 6 and 7, showing that three harmonics are present in the entire 0.8 second sample.

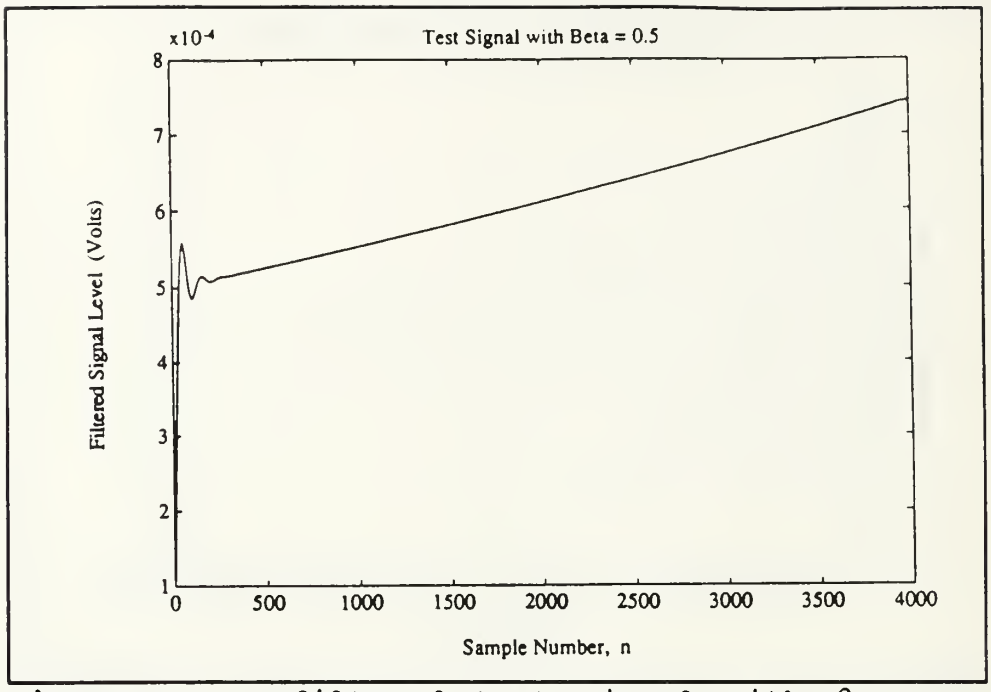

Figure 10 A filtered test signal with β = 0.5 showing the endpoint influence caused by the filter.

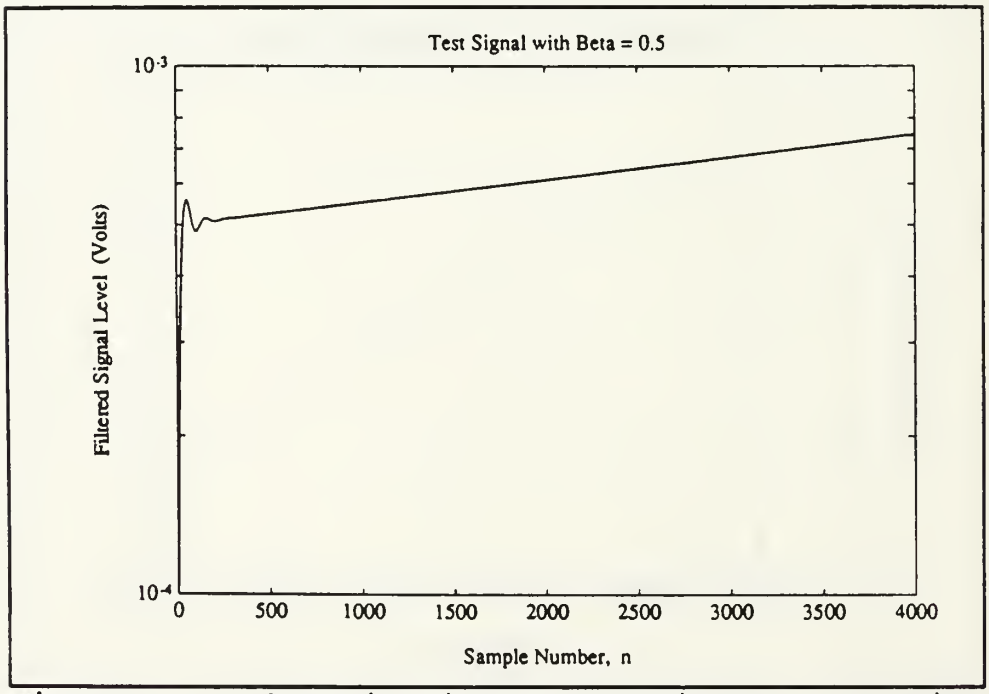

Figure 11 A logarithmic plot of Figure 10 showing the endpoint influence of the filter on a smooth test signal.

both the linear and logarithmic presentations for a test signal (β = 0.5) that was processed in accordance with the above procedure. As these plots indicate, the filter's endpoint effect extends to the first and last several hundred data points. To verify this, a least mean squares fit was applied to the natural logarithm of the test signal shown. In an attempt to eliminate the filter's endpoint effect the first and last 300 points were discarded. The result was that β could be determined to within one millionth of one percent, a negligible error. For data records which contained only the fundamental harmonic, this criteria of discarding the initial and final 300 data points, after filtering, was used to prevent the filter from adversely affecting the processed results.

In the case where a signal was observed to contain multiple harmonics, the filtered data was truncated at some value less than 3700. The actual value was determined by two criteria. First, as previously mentioned, the DFT was used to determine at what point in a data record, the buildup of the second harmonic began. This value marks the maximum acceptable truncation level. A least mean squares fit was then applied to the logarithm of the filtered signal truncated at this value. To evaluate the quality of this truncation, the filtered signal was plotted along with the least mean squares fit conducted over this truncated range. If the two curves did not visibly agree over the entire truncated range

then it was obvious that the fundamental was not completely isolated. This can occur because the initial buildup of a harmonic is difficult to detect. Because we are dealing with very narrow band frequencies, they will initially go undetected since the frequency bins are 1.25 hertz wide for a 0.8 second sample. Also, as less data is used in performing a DFT in an attempt to isolate the fundamental frequency, the frequency bins become wider. In cases where the results of the initial truncation were unsatisfactory, a smaller portion of the sample was chosen and the data was reprocessed under this same criteria until an agreement was evident. Appendix B gives a tabulation of each data record analyzed and the range of the points that were used for determining β.

This chosen segment of the filtered data record now represents the exponential behavior of the fundamental frequency alone and, assuming that $d\beta/dt$ is small, the natural log of this data is a line whose slope is equivalent to β. By performing a least mean squares fit to this data, a value for β can be obtained. Figures 12 through 15 show four typical data records. They reveal that β does not noticeably change over the time that the data is observed when only the first harmonic is present. The uncertainty in the slope was determined according to a procedure discussed in Beers' theory of errors (Beers, 1957). The maximum measurable error in all cases was only a small fraction of one percent.

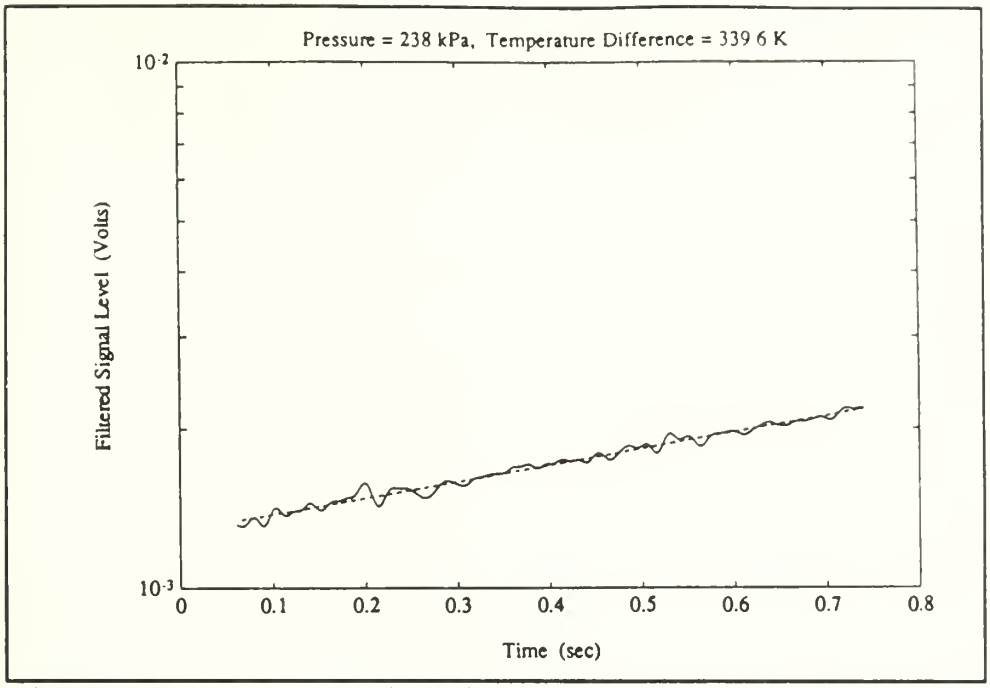

Figure 12 A logarithmic plot of a typical data record (solid line). The dashed line is a least mean squares fit of the data displayed.

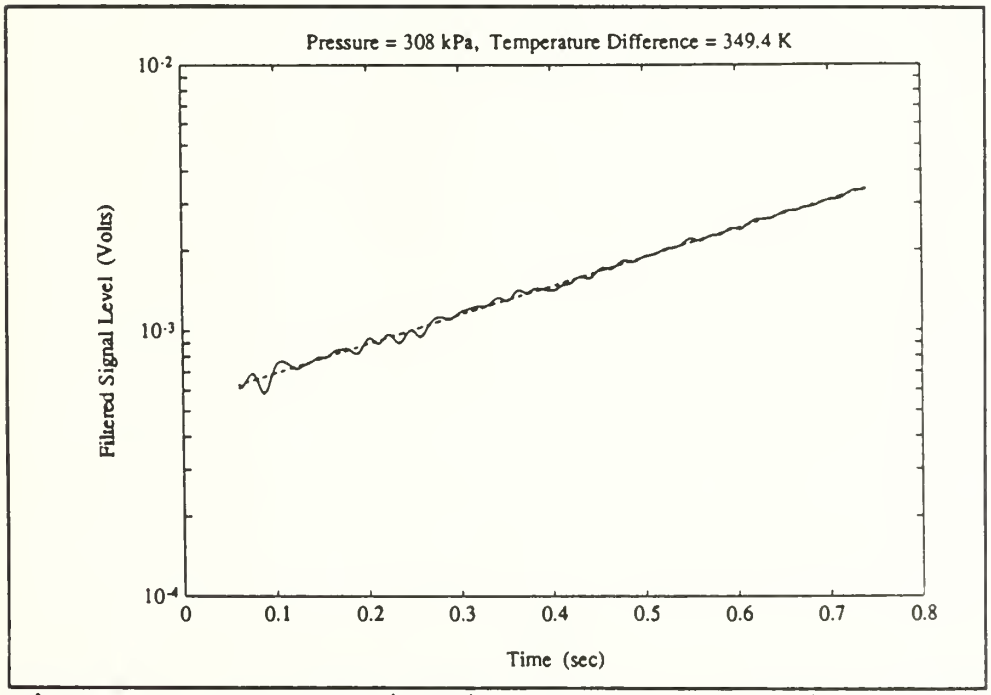

Figure 13 A logarithmic plot of a typical data record (solid line). The dashed line is a least mean squares fit of the data displayed.

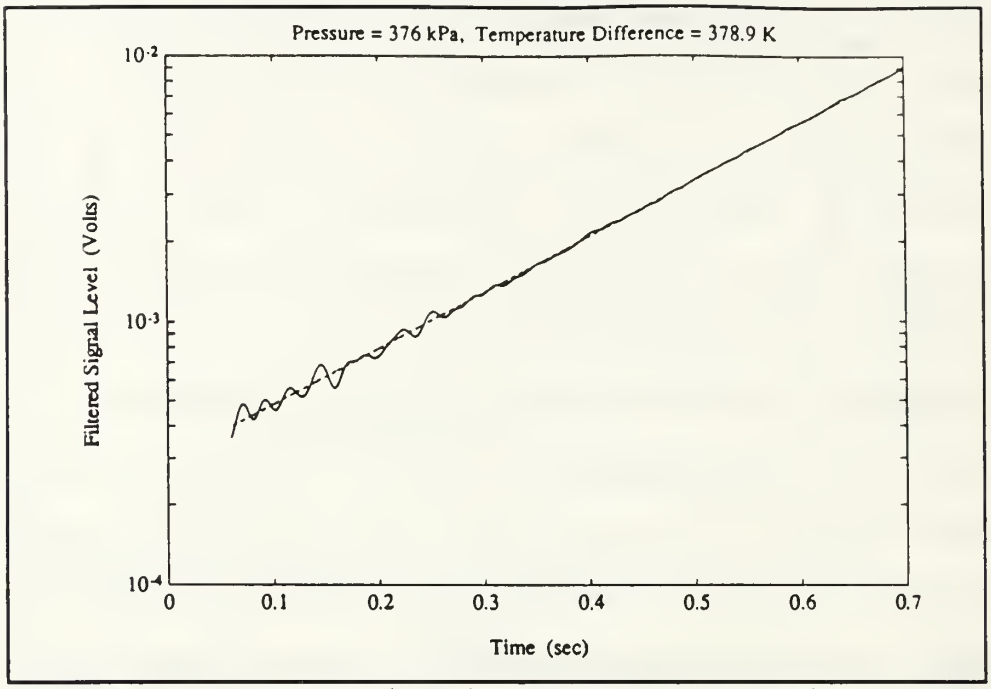

Figure 14 A logarithmic plot of a typical data record (solid line). The dashed line is a least mean squares fit of the data displayed.

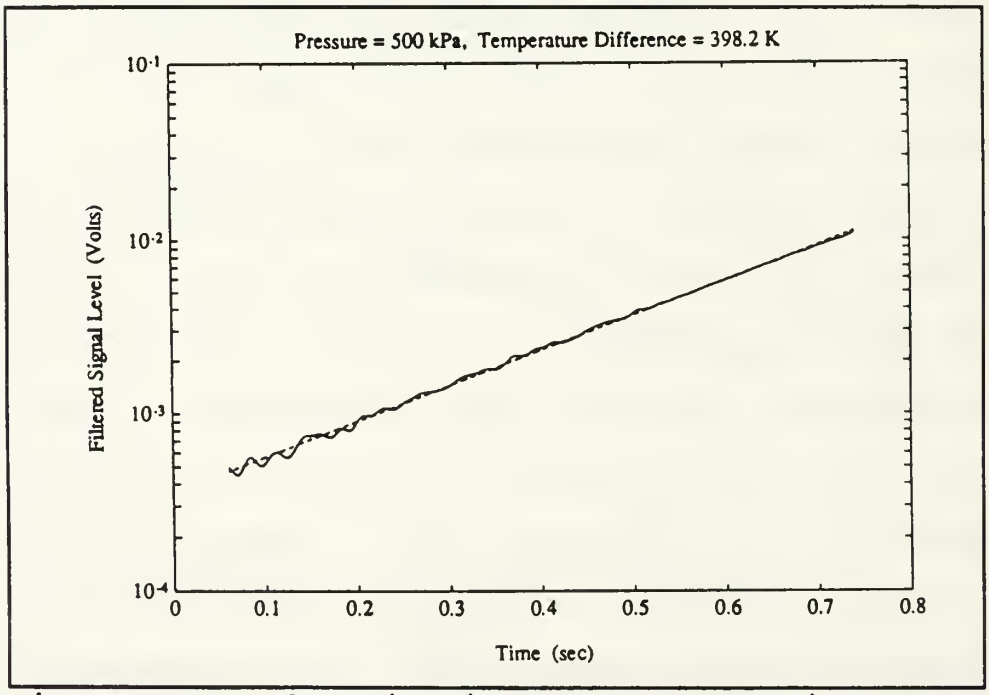

Figure 15 A logarithmic plot of a typical data record (solid line). The dashed line is a least mean squares fit of the data displayed.

V. RESULTS AND DISCUSSIONS

A. ABOVE ONSET DATA

Data was obtained for a helium filled prime mover above onset for mean gas pressures of 238, 308, 376, and 500 kPa, and differential temperatures ranging from onset up to approximately 400 K, in 10 degree increments. The pressures were chosen because they cover the range of the "ideal" gas pressure for the plate spacing in the prime mover stack and because they match the pressures analyzed in Lin's 1989 thesis. Although Lin also analyzed the pressure of 170 kPa, it was not used in this thesis. This is because the onset temperature of the prime mover at 170 kPa is so high that an insufficient range of data could be measured with a self imposed hot end temperature maximum of 700 K.

The results for the four pressures are presented in Figures 16 through 19 which show 1/Q as a function of the temperature difference across the stack. As can be seen, the collected data closely follows the slope of the theoretical curves and, for high mean gas pressure, the data and theory exactly agree. As the mean gas pressure decreases, however, the actual value at which onset occurs becomes increasingly higher than the theoretical value. Consequently, the spread between the actual data and the theory increases as well.

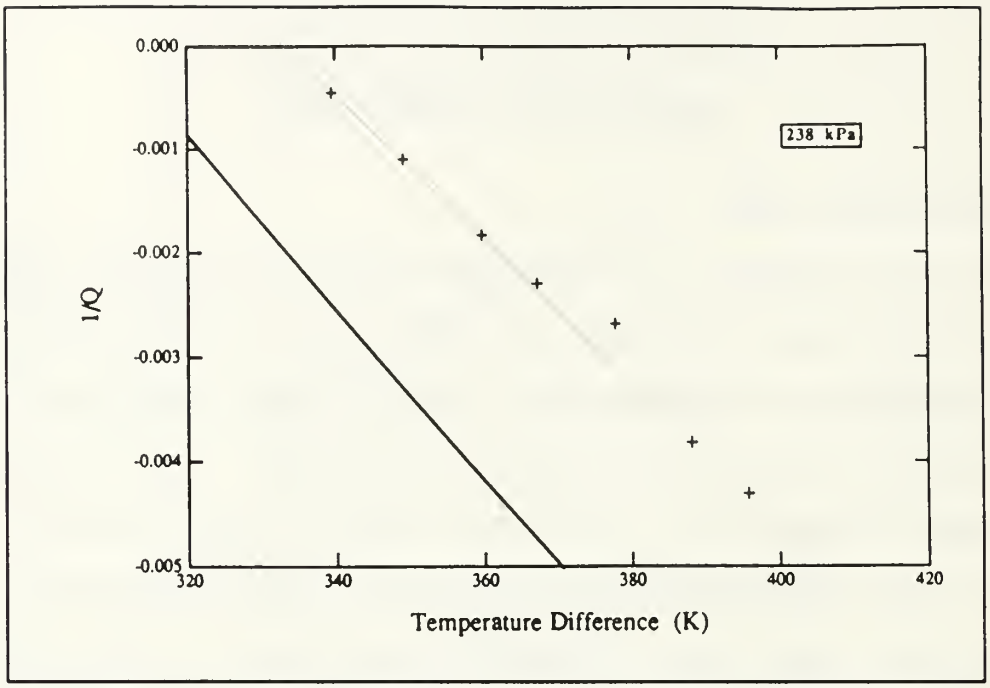

Figure 16 Data obtained for 238 kPa plotted as a function of the temperature difference across the stack. The solid line is the theoretical result.

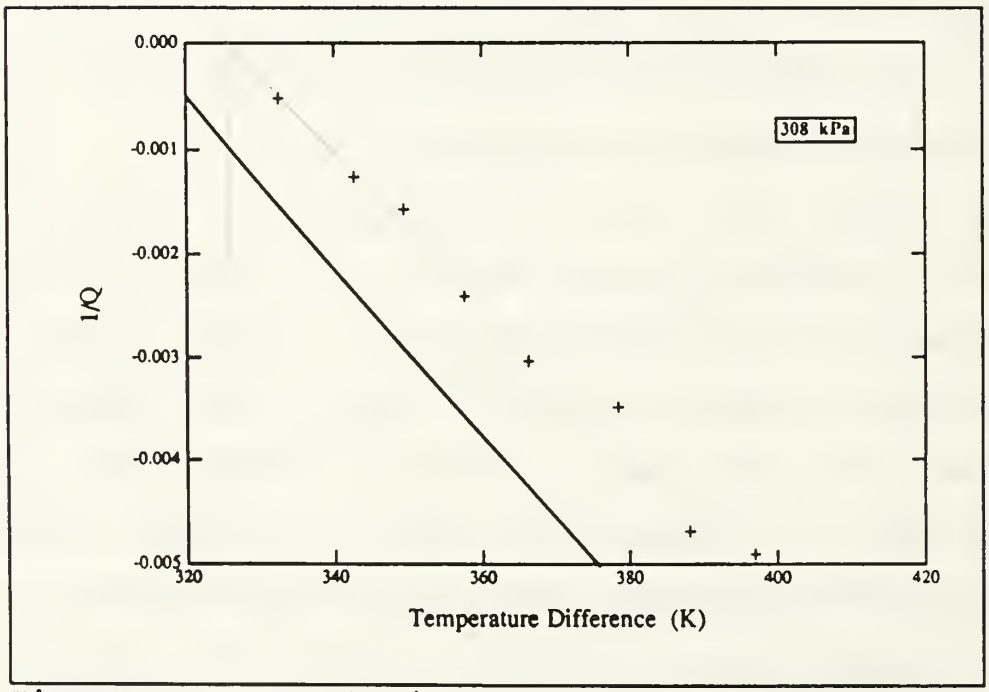

Figure 17 Data obtained for 308 kPa plotted as a function of the temperature difference across the stack. The solid line is the theoretical result.

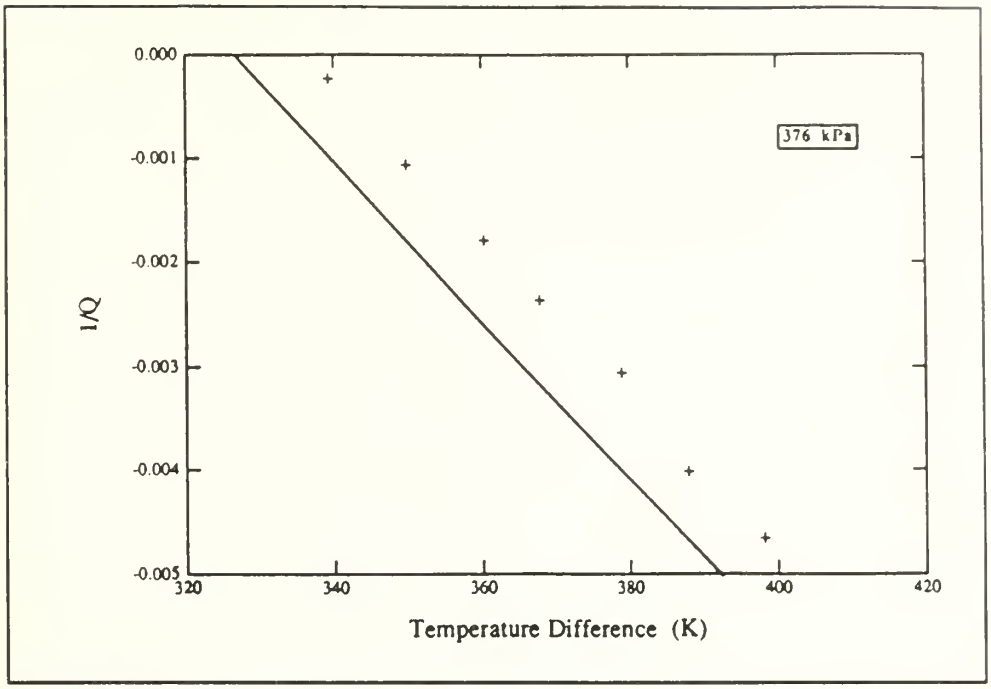

Figure 18 Data obtained for 376 kPa plotted as a function of the temperature difference across the stack. The solid line is the theoretical result.

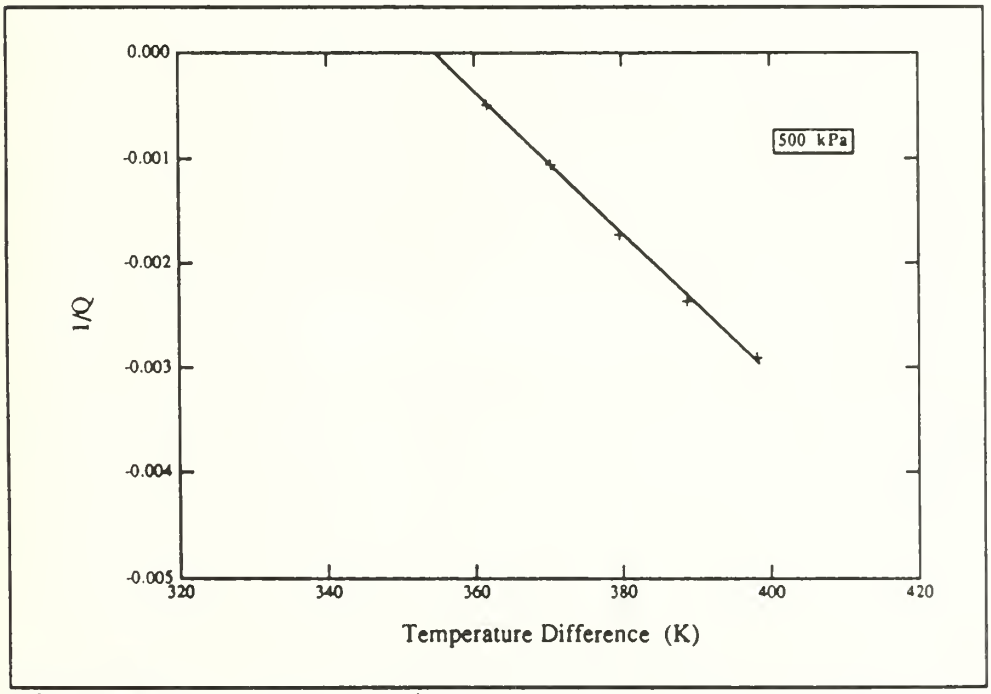

Figure 19 Data obtained for 500 kPa plotted as a function of the temperature difference across the stack. The solid line is the theoretical result.

The results can also be examined from a different point of view. Instead of an absolute comparison of theory and data, it is useful to consider 1/Q as a function of the number of degrees above onset. In this way, the actual results and the theory simply start from the common reference point of zero quality factor. This will consequently eliminate any discrepancies that result from failure to predict the precise onset temperature. Figures 20 through 23 present the data and the theory in this fashion. To determine the onset temperature for the measured data, a least mean squares fit was performed on the data and the result was extrapolated to find where 1/Q equaled zero. What these plots reveal is that at high mean gas pressures, theory exactly agrees with the measured data over the entire range of differential temperature measured (approximately 80 K). Again however, as the mean gas pressure decreases, the data visibly deviates from the expected theory within this differential temperature range observed.

Summarizing, the data displays two effects relating to the mean gas pressure. First, as the mean gas pressure decreases, the theoretical value of onset is increasing less than the measured value; and second, as the mean gas pressure decreases, the slope of the actual data is increasingly less than the theoretical slope. Three possible explanations exist as to why these deviations occur. First, imperfections in the construction of the prime mover may cause the prime mover's

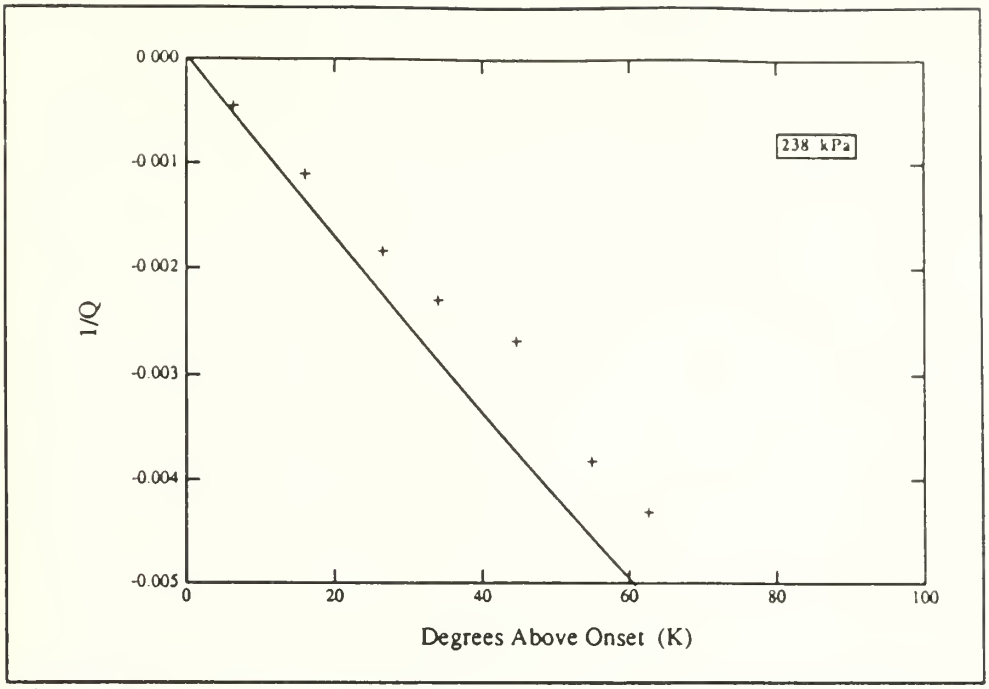

Figure 20 Data obtained for 238 kPa plotted as a function of the number of degrees above onset. The solid line is the theoretical result.

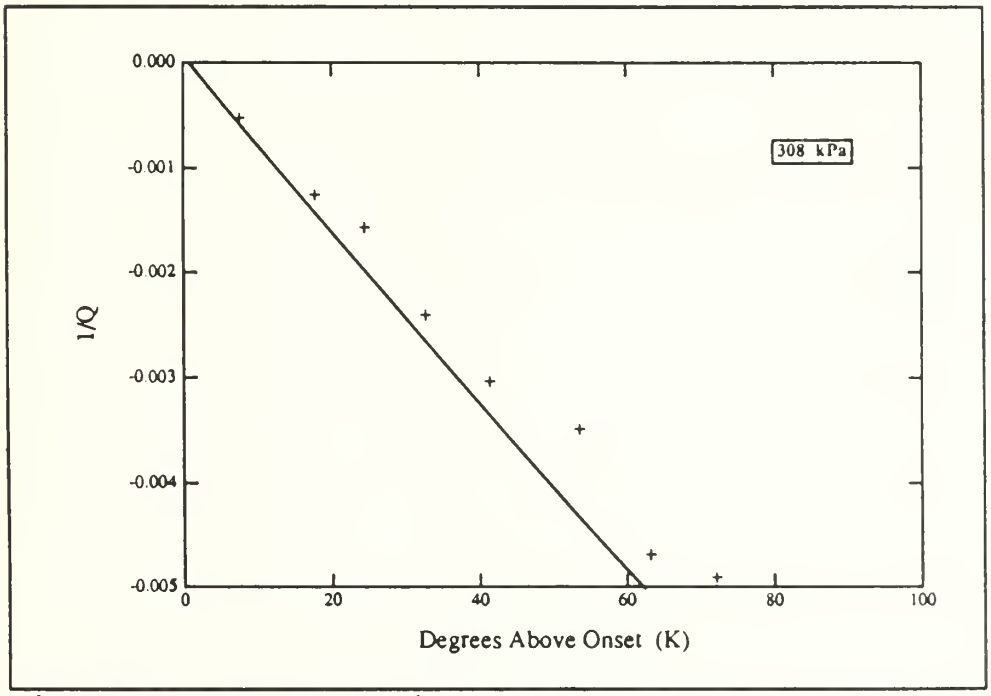

Figure 21 Data obtained for 308 kPa plotted as a function of the number of degrees above onset. The solid line is the theoretical result.

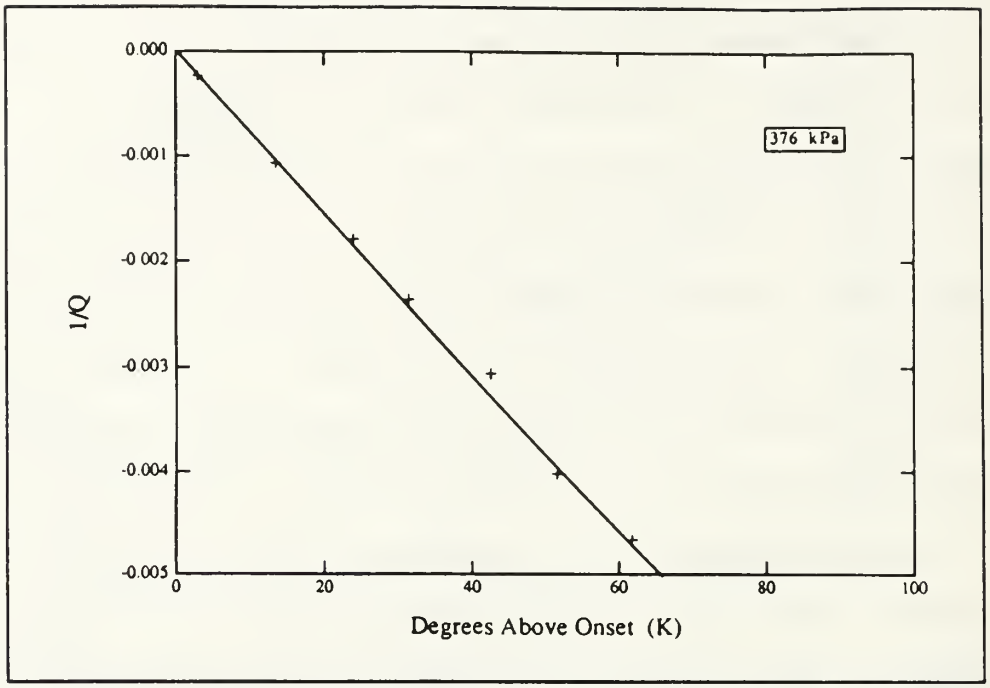

Figure 22 Data obtained for 376 kPa plotted as a function of the number of degrees above onset. The solid line is the theoretical result.

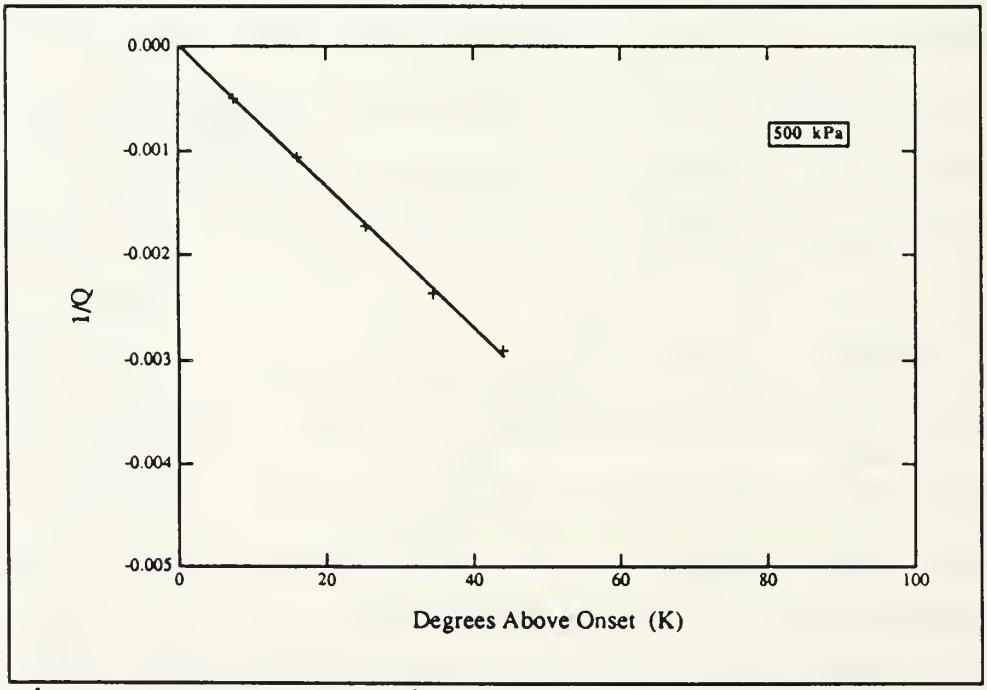

Figure 23 Data obtained for 500 kPa plotted as a function of the number of degrees above onset. The solid line is the theoretical result.

output to be less than ideal. Second, a difference in the rate of harmonic growth could be responsible for the data which is deviate from the theory. And third, the deviate data could have resulted if this data was measured during conditions of higher thermoacoustic heat transport.

Since the prime mover is not of ideal construction, its performance would be expected to be less than the theoretical prediction. This is what has been observed. In all cases, the measurements, at best, matched the theoretical results. The actual energy transport taking place in the prime mover stack occurs in a fluid channel which is approximately one thermal penetration depth thick (δ_κ) and centered approximately one thermal penetration depth from the plate (Swift, 1988, p.1152). This is important because as the mean gas pressure is decreased, δ_κ increases. Since δ_κ is also a function of temperature, its value changes along the stack. For the two lowest pressures looked at though, δ_κ at the average stack temperature, is greater than the half-gap spacing of the plates, and for the two highest pressures, it is smaller. Consequently, any imperfections in the arrangement of the plates would increasingly interfere with the prime mover's performance as the mean gas pressure is decreased. At higher mean gas pressures, the misalignment of the plates simply becomes less of a concern because the heat transport occurs closer to the plates.

The theory does not take into account energy lost to harmonics. So if harmonics are present, they would result in the absolute value of 1/Q being less that predicted. Analysis reveals, however, that harmonic growth is not the cause of the deviations. This is evident because the growth of higher harmonics was observed to be relatively independent of the mean pressure. Also, harmonic generation should be stronger for larger acoustic amplitudes. Therefore, it would reasonably be expected that the higher ΔT data would be more effected than the lower ΔT data since β is much larger. It can be seen however, from Figures 20 and 21, that the slope of the measured data, though in deviation with the theory, is very linear. No ΔT dependence is evident. Also, we were careful to exclude data records which had noticeable harmonic content.

Lastly, the question of heat transport must be addressed. The entire reason for looking at signals of low amplitude is to ensure that the heat transported by the sound is not yet significant. This is desired because, after the heat transport becomes significant, the heat exchangers initially have trouble keeping up with the energy demand placed upon them. The transport of heat through the fluid is simply faster than the transfer of energy through the solid heat exchangers. Consequently, the temperature of the hot and ambient end begin to change and the stack's condition becomes dynamic. With thermal equilibrium lost, the measured values

no longer represent β. Since heat transport is proportional to the square of the amplitude of the pressure wave, it is important to know at what pressure the signal was at when β was measured. Figures 24 through 27 show the range of the peak acoustic pressures generated by the prime mover in the data records used in determining the values of β. The pressures are small enough that the resultant heat transport is insignificant. Also, they are all approximately the same order of magnitude for the various mean pressures. As a result, any heat transport would be essentially the same for high and low mean pressures. Finally, deviations due to heat transport would be ΔT dependent because the pressure amplitudes are higher for higher values of ΔT. As noted above, however, no ΔT dependence is evident. It can be concluded therefore, that heat transport is not responsible for the deviations.

B. SOURCES OF ERROR

The theory discussed in Chapter II does not easily handle the insertion of the butterfly control valve in the prime mover ambient end. To see how much effect the valve has on Q, the Q of the prime mover was measured with no temperature difference applied to the stack. These results were then compared to Lin's measurements of Q for the same prime mover but without the valve. The measurement procedure used to obtain Q was identical to the procedure used by Lin in 1989.

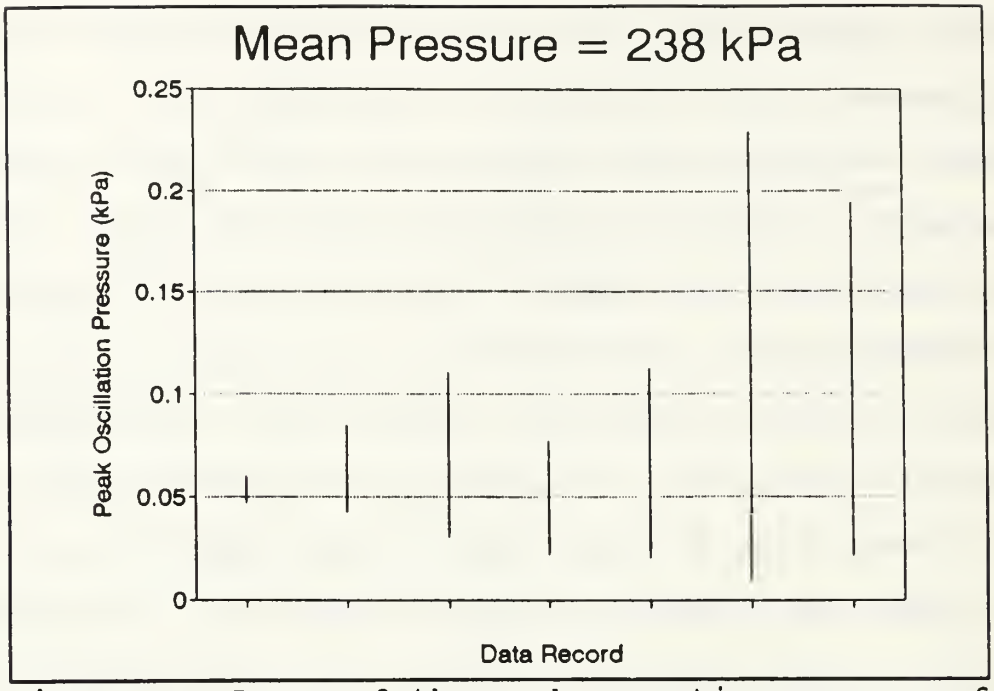

Figure 24 Range of the peak acoustic pressure of each data record used in determining β. (P = 238 kPa)

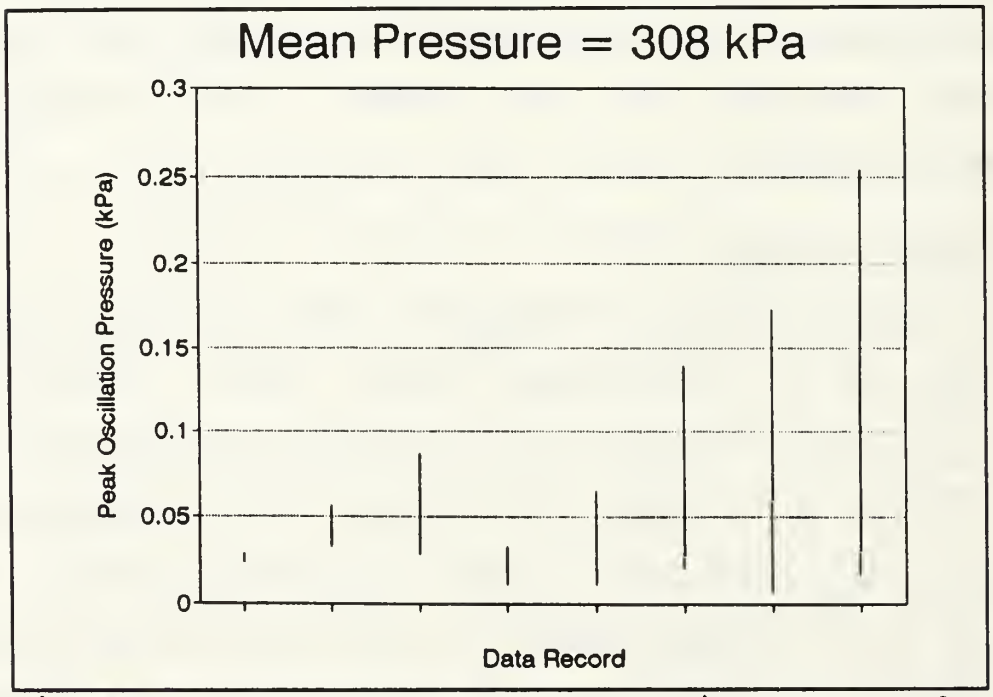

Figure 25 Range of the peak acoustic pressure for each data record used in determining β. (P = 308 kPa)

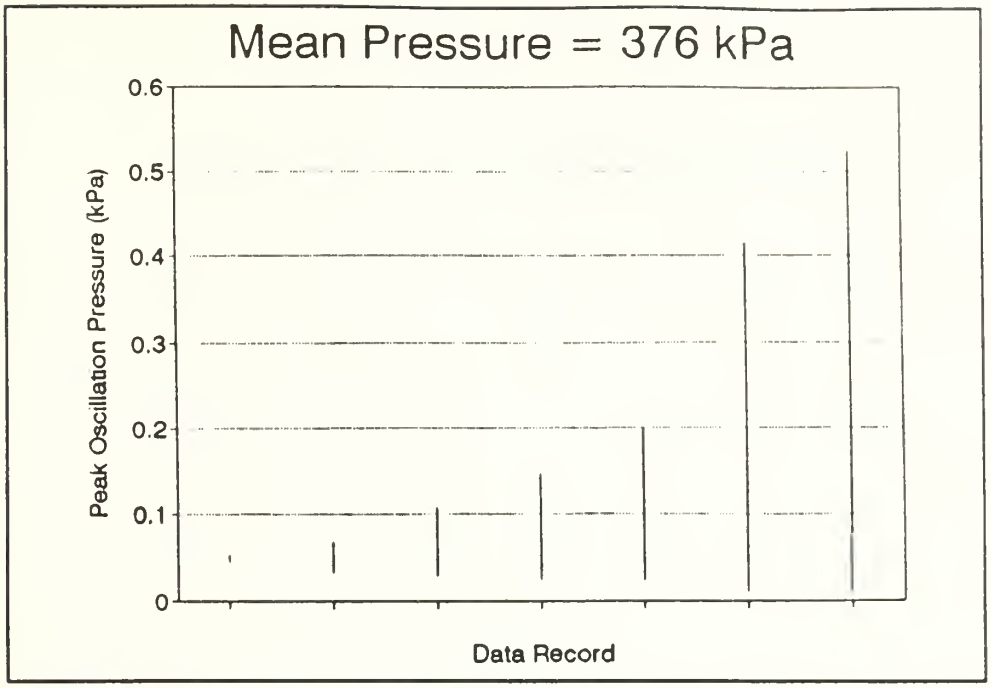

Figure 26 Range of the peak acoustic pressures for each data record used in determining β. (P = 376 kPa)

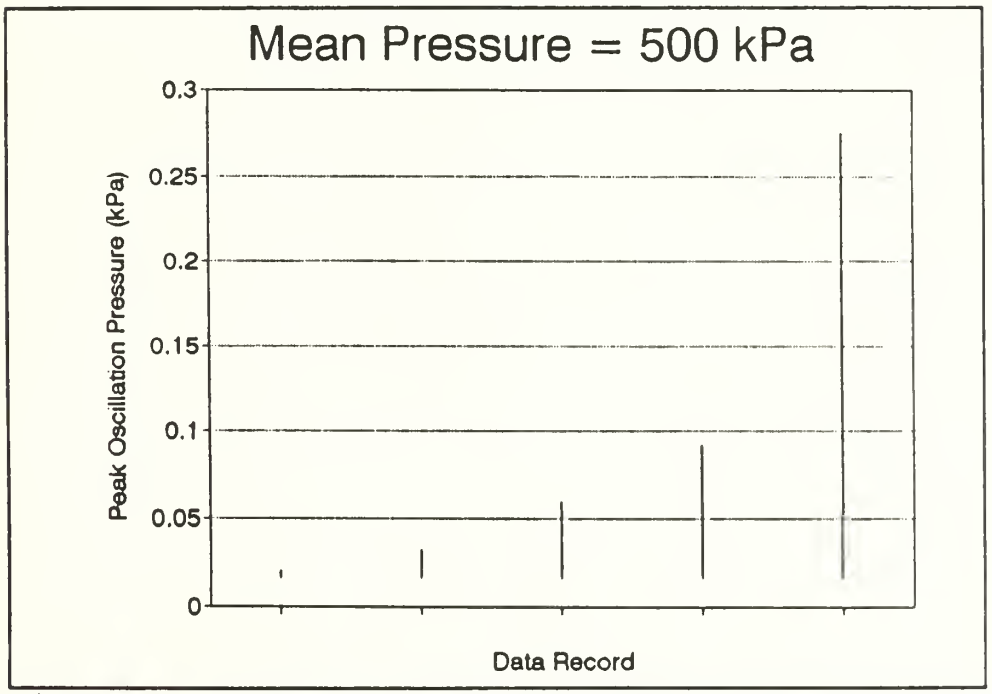

Figure 27 Range of the peak acoustic pressures for each data record used in determining β. (P = 500 kPa)

The results of this comparison show that the Q's agree within ~1%. (Lin, 1989, pp. 21-34)

The largest experimental error is likely due to the measurement in temperature. The error, based on manufacturer's specifications, is ±2°C for type E thermocouples and ±5°C for type K over the temperature range of interest.

As discussed at the beginning of Chapter IV, the error in mean pressure is ±1 kPa.

VI. CONCLUSIONS

It has been observed that the theoretical predictions of the work output of a prime mover are in very good agreement with the data for high mean gas pressures. As mean gas pressure decreases, however, the agreement diminishes. Likewise, the prediction of the slope of the data above onset is very good at high mean gas pressures. It is exact over large ranges of differential temperature. Again however, as the mean gas pressure decreases, the slope of the theoretical values of 1/Q increasingly exceed those of the experimental results. These results are consistent with those found for the same prime mover below onset (Lin, 1989). As explained in the previous chapter, these observed deviations are probably due to the inevitable construction irregularities of the prime mover stack. This method for measuring 1/Q has proven to be very effective for low amplitude signals.

To verify the discussion of the results in the previous chapter, it is recommended that one of two things be done. First, a working gas other than helium could be chosen. As a result, the thermal penetration depth δ_κ would be different from those employed in this thesis. If the same δ_κ to plate spacing ratios are examined as those in this thesis, then similar results are expected. Second, a new prime mover stack

could be constructed with a plate spacing different from that of the stack used here. When analyzed at pressures that give the same penetration depth to plate spacing ratio, similar results are expected. If either experiment produces results that differ from those seen here, then it would indicate that the source of the deviations observed in this thesis is something more than just a physical construction problem.

APPENDIX A

PRIME MOVER DIMENSIONS

Prime Mover Internal Length	Prime Mover Internal Radius
100.05 cm	1.91 cm

COMPONENT DIMENSIONS AND LOCATIONS

Component	Ambient Heat Exchanger	Stack	Hot Heat Exchanger
Width (Δx)	2.18* cm	3.50 cm	0.762 cm
Plate half-gap (y_o)	0.052 cm	0.0385 cm	0.052 cm
Plate half-thickness (l)	0.0225 cm	0.014 cm	0.0225 cm
Total plate perimeter	312 cm	206 cm	156 cm
Location (x)	88.11 cm	90.29 cm	93.79 cm

* Includes 0.15 cm gap between twin heat exchangers.

APPENDIX B

DATA RECORD SUMMARY

Pressure(kPa)	Temperature Difference(K)	Range containing only first harmonic	Filtered range used in β measurement
238	339.6	1-4000	300-3700
238	349.2	1-3000	300-3000
238	359.7	1-4000	300-3700
238	367.2	1-4000	300-3700
238	378.4	1-3000	300-2000
238	388.1	1-3000	300-3000
238	349.4	1-2000	300-2000
308	332.5	1-4000	300-3700
308	342.7	1-4000	300-3700
308	349.4	1-4000	300-3700
308	357.6	1-4000	300-3000
308	366.3	1-4000	300-3700
308	378.4	1-4000	300-3700
308	349.4	1-3000	300-3000
308	397.0	1-2000	300-1500

DATA RECORD SUMMARY (CONTINUED)

Pressure(kPa)	Temperature Difference(K)	Range containing only first harmonic	Filtered range used in β measurement
376	339.3	1-4000	300-3700
376	360.3	1-3000	300-3700
376	360.3	1-3000	300-3700
376	367.8	1-3000	300-3700
376	378.9	1-3000	300-3500
376	387.9	1-4000	300-2000
376	398.1	1-3000	300-2000
500	361.7	1-3000	300-3700
500	370.9	1-4000	300-3700
500	379.6	1-4000	300-3700
500	388.7	1-3000	300-3700
500	398.2	1-4000	300-3700

APPENDIX C

EQUATIONS USED FOR DETERMINING TEMPERATURE DEPENDENT QUANTITIES

Mean Temperature as a function of x:

$$T_m[x] = k_{T0} + k_{T1}(x - x_{stack}) + k_{T2}(x - x_{stack})^2$$

$$k_{T0} = c_{T00} + c_{T01}\Delta T$$
$$k_{T1} = c_{T10} + c_{T11}\Delta T + c_{T12}(\Delta T)^2$$
$$k_{T2} = c_{T20} + c_{T21}\Delta T + c_{T22}(\Delta T)^2$$

$$c_{T00} = 292.86$$
$$c_{T01} = 0.00171124$$

$$c_{T10} = -12.6165$$
$$c_{T11} = 29.0362$$
$$c_{T12} = 0.00920377$$

$$c_{T20} = 335.803$$
$$c_{T21} = -12.3295$$
$$c_{T22} = -0.270547$$

Mean Temperature Gradient:

$$\nabla T_m[x] = k_{g0} + k_{g1}e^{-k_{g2}(x - x_{stack})}$$

$$k_{g0} = c_{g00} + c_{g01}\Delta T + c_{g02}(\Delta T)^2$$
$$k_{g1} = c_{g10} + c_{g11}\Delta T + c_{g12}(\Delta T)^2$$
$$k_{g2} = c_{g20} + c_{g21}\Delta T + c_{g22}(\Delta T)^2$$

$$c_{g00} = 9.36469$$
$$c_{g01} = 18.9501$$
$$c_{g02} = 0.0000435077$$

$$c_{g10} = -9.90268$$
$$c_{g11} = 9.63328$$
$$c_{g12} = 0.0122971$$

$$c_{g20} = 0.121556$$
$$c_{g21} = 0.0722492$$
$$c_{g22} = -0.0000210737$$

Sound Speed:

$$a[T] = a_o \sqrt{T/T_o}$$

$$a_o = 1008 \ m/s$$
$$T_o = 293 \ K$$

Angular Frequency:

$$\omega[\Delta T] = \frac{n\pi}{\frac{x_{stack}}{a[T_{amb}]} + \omega_1[x_{stack}+\Delta x_{stack}] + \frac{(1 - x_{stack} - \Delta x_{stack})}{a[T_{hot}]}}$$

$$\omega_1[x] = 2\sqrt{T_o}\left[\sqrt{T_{amb} + \nabla T[x]\,(x - x_{stack})} - \sqrt{T_{amb}}\right] - \frac{\sqrt{T_{amb}}}{a_o \nabla T[x]}$$

Phase:

$$\phi[x] = \phi_1[\Delta T]\left[\sqrt{T_{amb} + \nabla T[x]\,(x - x_{stack})} - \sqrt{T_{amb}}\right]$$

$$\phi_1[\Delta T] = 2\omega[\Delta T]\sqrt{T_o}/(a_o \nabla T[x])$$

Miscellaneous:

$$k[T] = \omega[\Delta T]/a[T]$$

$$\mu[T] = \mu_o (T/T_o)^{\beta}$$

$$\kappa[T] = \kappa_o (T/T_o)^{\beta}$$

$$\rho_m[T] = \rho_o (P/P_o)\,(T_o/T)$$

$$\delta_\kappa[T] = \sqrt{2\kappa[T]/(\rho_m[T]\, c_{p_o}\, \omega[\Delta T])}$$

$$\delta_v[T] = \sqrt{2\mu[T]/(\rho_m[T]\, \omega[\Delta T])}$$

$$\sigma[T] = (\delta_v[T]/\delta_\kappa[T])^2$$

Miscellaneous (continued):

$$\beta = 0.694$$
$$\gamma = 5/3$$
$$\mu_o = 1.961\times10^{-6} \quad Pa\cdot sec$$
$$\kappa_o = 0.1524 \quad W/m\cdot K$$
$$\rho_o = 0.164 \quad kg/m^3$$
$$P_o = 1.01\times10^{5} \quad Pa$$
$$c_{p_o} = 5197 \quad J/kg\cdot K$$

LIST OF REFERENCES

Beers, V., Introduction to the Theory of Errors, Addison-Wesley, 1957.

Garrett, S. L., and Gabrielson, T. B., "Magnetohydrodynamic and Thermoacoustic Mechanisms for Generation of Sound in Seawater," Power Transducers for Sonics and Ultrasonics, Springer-Verlag, 1991.

Lin, Hsiao-Tseng, Investigation of a Heat Driven Thermoacoustic Prime Mover, Master's Thesis, Naval Postgraduate School, Monterey, California, December 1989.

Strum, Robert D., and Kirk, Donald E., First Principles of Discrete Systems and Digital Signal Processing, Addison-Wesley, 1988.

Swift, G. W., "Thermoacoustic engines," J. Acoust. Soc. Am. Vol. 84, October 1988.

INITIAL DISTRIBUTION LIST

1.	Defense Technical Information Center Cameron Station Alexandria, VA 22304-6145	2
2.	Library, Code 0142 Naval Postgraduate School Monterey, CA 93943-5002	2
3.	Prof. A. Atchley, Code PH/Ay Physics Department Naval Postgraduate School Monterey, CA 93943	5
4.	Dr. Felipe Gaitan, Code PH Physics Department Naval Postgraduate School Monterey, CA 93943	1
5.	Dr. Logan E. Hargrove Office of Naval Research Physics Division - Code 1112 800 N. Quincy Street Arlington, VA 22217-5000	1
6.	Dr. Henry E. Bass Physical Acoustics Research Laboratory University of Mississippi University, MS 38677	1
7.	Prof. J. Miller Electrical and Computer Engineering Department Code EC/Mr Naval Postgraduate School Monterey, CA 93943	1
8.	LT. Earl C. Bowers, USN 12018 N.E. Lonetree Ct. Poulsbo, WA 98370	2

Thesis
B7483 Bowers
c.1 Investigation of a heat driven thermoacoustic prime mover above onset of self-oscillation.